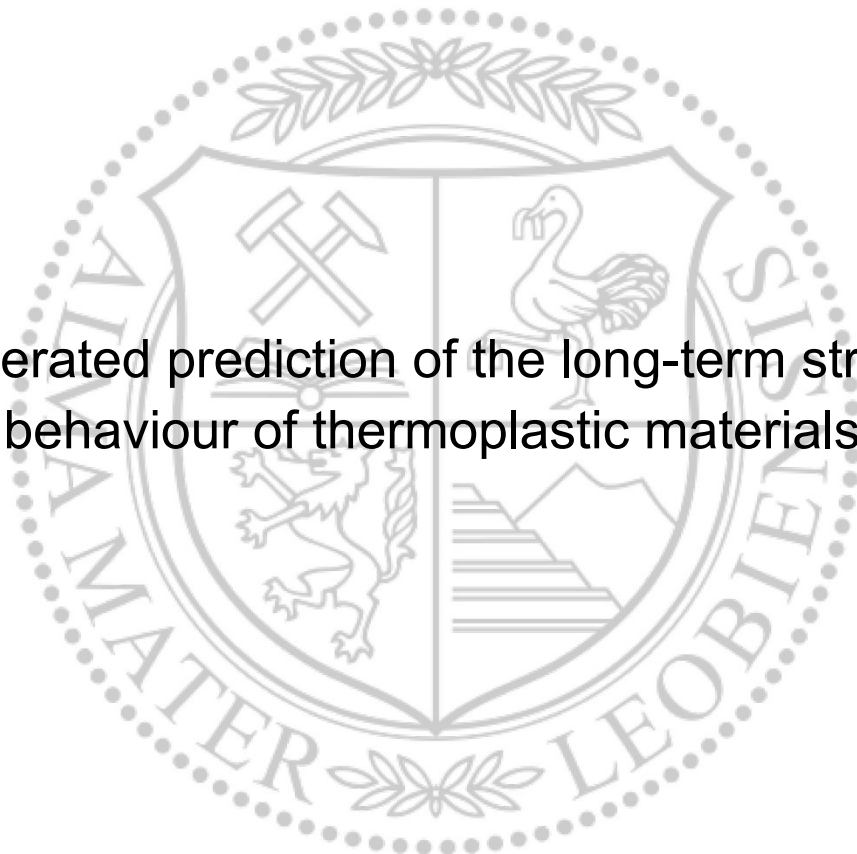




Chair of Materials Science and Testing of Polymers

Master's Thesis

Accelerated prediction of the long-term strength  
behaviour of thermoplastic materials



Jessica Hinczica, BSc

March 2020

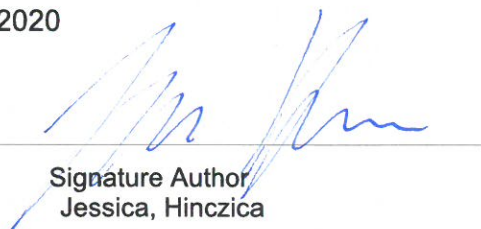
**AFFIDAVIT**

I declare on oath that I wrote this thesis independently, did not use other than the specified sources and aids, and did not otherwise use any unauthorized aids.

I declare that I have read, understood, and complied with the guidelines of the senate of the Montanuniversität Leoben for "Good Scientific Practice".

Furthermore, I declare that the electronic and printed version of the submitted thesis are identical, both, formally and with regard to content.

Date 08.03.2020



---

Signature Author  
Jessica, Hinczica

## **ACKNOWLEDGEMENTS**

First of all, I would like to thank all people, who supported me during the progression of this thesis and my studies at Montanuniversitaet Leoben.

I would like to thank Univ.-Prof Dr. Gerald Pinter (Chair of Materials Science and Testing of Polymers, Montanuniversitaet Leoben) for making this master thesis possible and for his review. He supported me in understanding difficult issues and enabled to perform all necessary measurements on the machines at the Chair. Special thanks go to my supervisor Dipl.-Ing. Dr. mont. Gerald Pilz, who always supported me in planning and executing the thesis. His knowledge and involvement in the development of the SRCR-test enabled him to contribute his expertise to the modification of the test. Among other things I thank him for correcting and evaluating my thesis.

I am particularly grateful to my supervisor Dipl.-Ing. Mario Messiha, for his support at the Polymer Competence Center Leoben GmbH (PCCL). He always guided me and took time to discuss and explain various topics. Because of his critical assessment and his patience, he passed on a lot of knowledge to me.

I am also in debt of Dipl.-Ing. Dr. mont. Andreas Frank, who enabled me to create this thesis and gave me further education in his working group. Above all, I am grateful for the commitment he shows to his students. In special, I am glad that my colleague Herbert Fladenhofer supported me during the measurements and also mentally.

The present thesis was part of the COMET-project "Development of polyethylene with superior properties for extended pipe applications" (Project-No.: VI-3.08a) at the Polymer Competence Center Leoben GmbH within the competence center program COMET of the Federal Ministry of Transport, Innovation and Technology and Federal Ministry of Science, Research and Economy with the participation of the Montanuniversitaet Leoben, Department of Materials Science and Testing of Polymers as well as SCG Chemicals Co., Ltd (Thailand). The PCCL is funded by the federal government and the states of Styria, Lower Austria and Upper Austria.

Last but not least, I would like to express my deepest gratitude to my family, my parents Edith and Karl, my siblings Florian and Vanessa and my grandparents Anneliese and Karl. They made it possible for me to study at Montanuniversitaet Leoben and to spend an exciting semester abroad. Through their infinite love they supported me in every situation in life and helped me wherever possible. Without them I would not be the person I am today. THANK YOU!

## ABSTRACT

In the present thesis, a method has been modified to predict the long-term strength behaviour of thermoplastic materials. The method is based on the Stress-Rate accelerated Creep Rupture (SRCR) test, which was previously developed for brittle materials and which was transferred to tough materials within this thesis. For this purpose, monotonic tests under different loading rates were carried out at room temperature as well as at elevated temperature. These tests were performed at various specific reference stresses and stress rates. By varying the stress rates from high to low, the time to failure was extrapolated to a stress rate of 0 MPa/s, which corresponds to a static test at the specific reference stress level. A conservative approach was chosen for the evaluation, in which yielding is considered as total failure. The extrapolation was evaluated using the determined yield stresses and the corresponding time until the yield stress occurs. Also, the linear dependence of the failure behaviour (in this particular case the yield stress) on the stress rate and the temperature was determined to allow extrapolation of the failure behaviour. This correlation is given for all materials, where the yield stress increases with increasing stress rate. The adaptation was performed on four conventional pipe materials - a polyamide 12 (PA12) with a minimum required strength (MRS) of 18 MPa, and three high-density polyethylene types (PE-HD), MRS = 10 MPa.

The modified SRCR test has a high potential for predicting the long-term strength of thermoplastic materials. Due to some experimental conditions (temperature and stress rate) it is difficult to identify the yield stress, so this method has its limitations in the evaluation, particularly at high temperature ranges and low stress rates. Limitations were determined especially for PA12 – the stress rate should be  $\geq 0.001$  MPa/s and the temperature  $< 80$  °C, to allow a sufficient reproducibility. Static long-term measurements (e.g. creep tests) should be conducted to additionally support the accuracy of the accelerated prediction.

## KURZFASSUNG

In der vorliegenden Arbeit wurde eine Methode modifiziert, um das Langzeitverhalten von thermoplastischen Materialien vorherzusagen. Die Methode basiert auf dem SRCR-Test, der für spröde Materialien entwickelt wurde und auf zähe Materialien übertragen werden soll. Dazu wurden monotone Tests unter verschiedenen Belastungsraten bei Raumtemperatur als auch bei erhöhter Temperatur durchgeführt. Diese Versuche wurden bei verschiedenen spezifischen Referenzspannungen und Spannungsraten durchgeführt. Durch Variation der Spannungsraten (von hoch bis niedrig) kann die Zeit bis zum Versagen auf eine Spannungsrate von 0 MPa/s extrapoliert werden, was einem statischen Versuch bei der spezifischen Referenzspannung entspricht. Für die Auswertung wurde ein konservativer Ansatz gewählt, bei dem das Fließen als Totalversagen betrachtet wird. Die Extrapolation wurde unter Verwendung der ermittelten Fließspannungen und der entsprechenden Zeit bis zum Auftreten der Fließspannung ausgewertet. Außerdem wurde die lineare Abhängigkeit des Versagensverhaltens (in diesem Fall die Fließspannung) von der Spannungsrate und der Temperatur bestimmt, um eine Extrapolation des Versagensverhaltens zu ermöglichen. Diese lineare Abhängigkeit ist für alle Werkstoffe gegeben, die Fließspannung steigt mit zunehmender Spannungsrate, eine lineare Regression kann durchgeführt werden. Die Modifizierung wurde an vier konventionellen Rohrmaterialien durchgeführt - einem Polyamid 12 (PA12) mit einer minimal erforderlichen Festigkeit (MRS) von 18 MPa und drei high-density Polyethylen (HDPE), MRS = 10MPa. Für eine beschleunigte Vorhersage wurden zusätzliche Messungen bei  $T = 80^{\circ}\text{C}$  durchgeführt.

Der modifizierte SRCR-Test hat ein hohes Potenzial für die Vorhersage der Langzeitfestigkeit von thermoplastischen Materialien. Aufgrund experimenteller Bedingungen (Temperatur und Spannungsrate) ist es schwierig, die Fließspannung zu bestimmen, so dass diese Methode ihre Grenzen in der Auswertung hat, insbesondere bei der Auswertung bei hohen Temperaturen und bei niedrigen Belastungsraten. Die Grenzen traten speziell bei PA12 auf, die Spannungsrate sollte  $\geq 0,001$  MPa/s und die Temperatur  $< 80^{\circ}\text{C}$  betragen, um eine Auswertung nach dieser Methode zu ermöglichen. Statische Langzeitmessungen (z.B.

Kriechversuche) können die Genauigkeit der beschleunigten Vorhersage zusätzlich unterstützen.

**TABLE OF CONTENTS**

<b>AFFIDAVIT</b> .....	<b>I</b>
<b>ACKNOWLEDGEMENTS</b> .....	<b>II</b>
<b>ABSTRACT</b> .....	<b>IV</b>
<b>KURZFASSUNG</b> .....	<b>V</b>
<b>TABLE OF CONTENTS</b> .....	<b>VII</b>
<b>1 INTRODUCTION</b> .....	<b>1</b>
<b>2 BACKGROUND</b> .....	<b>2</b>
2.1 POLYAMIDE & POLYETHYLENE PIPE GRADES .....	2
2.2 FAILURE BEHAVIOUR OF PRESSURIZED POLYMER PIPES .....	4
2.2.1 Deformation processes of yielding in semi-crystalline Polymers .....	6
2.2.2 Eyring Theory .....	7
2.2.3 Kinetic Fracture Theory .....	10
2.3 ACCELERATED METHODS FOR LONG-TERM FAILURE PREDICTION .....	11
2.3.1 SRCR-Test .....	12
2.3.2 Accelerated long-term plasticity-controlled test.....	13
2.4 EQUIVALENT STRESS HYPOTHESES.....	15
2.4.1 Maximum stress criterion according to von Mises .....	16
2.4.2 Maximum shear criterion according to Tresca .....	16
<b>3 EXPERIMENTAL</b> .....	<b>17</b>
3.1 MATERIALS .....	17
3.2 BASIC MATERIAL CHARACTERIZATION .....	17
3.2.1 Density.....	17
3.2.2 Melt Flow Rate .....	18
3.2.3 Differential Scanning Calorimetry.....	18
3.2.4 Tensile Tests .....	19
3.3 MODIFICATION OF THE SRCR-TEST.....	19



---

<b>4</b>	<b>RESULTS AND DISCUSSION.....</b>	<b>24</b>
4.1	BASIC MATERIAL PROPERTIES.....	24
4.1.1	Density and Melt Flow Rate .....	25
4.1.2	Differential Scanning Calorimetry.....	25
4.1.3	Tensile Tests .....	26
4.2	LONG TERM CREEP RUPTURE BEHAVIOUR .....	28
4.3	COMPARISON TO INTERNAL PIPE PRESSURE TEST .....	40
<b>5</b>	<b>SUMMARY.....</b>	<b>45</b>
<b>6</b>	<b>PUBLICATION BIBLIOGRAPHY .....</b>	<b>47</b>

## 1 INTRODUCTION

The expectations of polymers in the various fields of application are constantly increasing. The lifetime under a static load is highly relevant. Many polymers are available for long-term application. Due to the excellent properties of polyamide 12 (PA12) and high-density polyethylene (HDPE), the materials are used in pipe application. The high strength and stiffness and also the resistance to corrosion of PA12 make this material suitable for gas pipe applications. Both in terms of chemical resistance and mechanical properties, PE has been used for decades for water and gas distribution systems. For pipe application, requirements and lifetime are high. The determination of this long-term strength performance of these materials is based on internal pipe pressure tests according ISO 9080 and ASTM D2837 (Hydrostatic Design Basis, HDB), respectively. A pipe is loaded with an internal stress until failure occurs. These testing methods are very expensive and time-consuming with testing times up to  $10^4$  h. Therefore, alternative accelerated methods are of high interest.

Regarding composite materials a new approach has been developed recently, which allows an extrapolation of the long-term creep rupture by applying a variety of stress-rates. This so-called Stress-Rate accelerated Creep Rupture (SRCR) test (Gloggnitzer et al., 2018) is practicable within only a couple of days. Results of the SRCR-test of relatively stiff and brittle composites are in good accordance to classical long-term creep rupture tests. However, for thermoplastic materials of relatively low stiffness and higher toughness, which are used for polymer pipes, the SRCR-test has not been sufficiently adapted yet.

The main focus of this master thesis is the evaluation of the applicability and the development of suitable test parameters for the SRCR-test for thermoplastic pipe grades. Dependencies of the measured properties on the different testing parameters are also determined and explained. The SRCR-test is based on phenomenological approaches; by examining the different dependencies it is to be determined whether this test is also applicable to the plasticity of tough materials.

## 2 BACKGROUND

In the following sections the basics of this thesis are explained. At the beginning, the materials PA and PE are discussed. Then the focus is on the failure behaviour of pressurized polymer pipes and especially the physical processes of the relevant failure mechanism. Finally, two accelerated methods for the long-term failure prediction are introduced in more detail and the comparison of uniaxial and multiaxial tests using equivalent stresses is explained.

### 2.1 Polyamide & Polyethylene Pipe Grades

For decades, in addition to metallic materials, thermoplastic materials have been used as pipe materials. From the group of polyolefins, PE, especially high-density PE (HDPE) is the most commonly used material and is mainly applied for water distribution systems. For gas pipe applications at higher pressures (around 18 bar) HDPE is no longer suitable and metallic materials are used. Recently, the chemical and corrosion resistant PA12 is used as an alternative to metallic materials for applications at higher pressures. Pipes made of PA12 do not require additional corrosion protection and can be rolled-up, which simplifies transport and reduces the number of weldings (Hartmann, 2014).

High strength, stiffness and hardness as well as good deformation resistance in heat and resistance to solvents and fuels characterize the properties of PA. However, the high affinity to water absorption is the significant disadvantage of these materials. Extensive adaption to the respective requirements can be achieved by selecting different types. These types differ in the monomer used and the resulting structure of the polymer. The influence of the manufacturing conditions on the crystallinity of PA is high, with increasing crystallinity, water absorption decreases and the mechanical properties improve. The properties are determined by the amide group CO-NH, the higher the number of amide groups, the higher the melting point and the affinity to water absorption. For pipe applications, a semi-crystalline aliphatic PA12, produced by polycondensation of Laurolactam is used. The monomer and the polymer unit are shown in Fig. 2.1. This PA12 is distinguished by its very low water absorption, good impact strength compared to other PA types and is also

resistant to stress corrosion. It is a tough material with a high stiffness and a density of  $>1000 \text{ kg/m}^3$ . Material properties of PA12 are summarized in Table 2.1 (Domininghaus et al., 2012; Bonten, 2016).

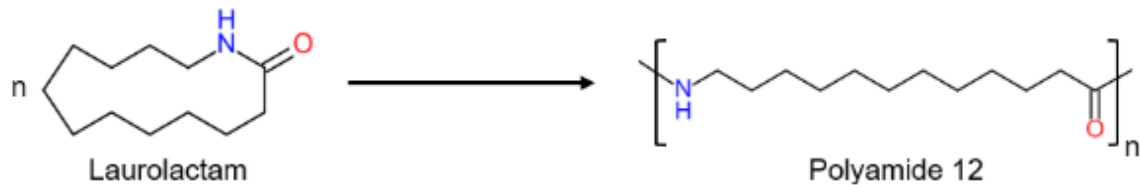


**Fig. 2.1:** Polymerization of PA12 from Laurolactam (Domininghaus et al., 2012).

Various types of PE are realized by different polymerization of Ethylene (Fig. 2.2). These differ mainly in the molecular structure (degree of branching) and density. A difference is made between unbranched, short-chain-branched and long-chain-branched molecular chains. Pipe grades used today are HDPE, produced at lower temperature  $T$  and pressure  $p$  than low density PE (LDPE).

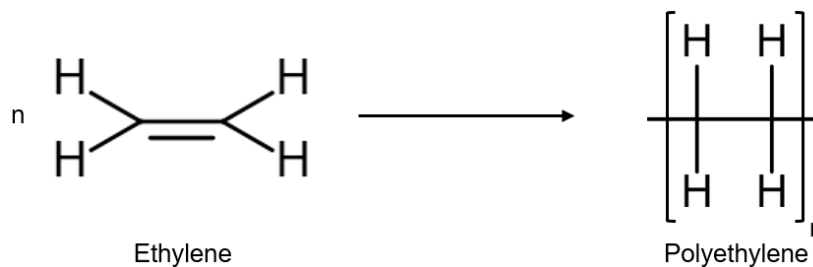


**Fig. 2.2:** Polymerization of PE from Ethylene (Brömstrup, 2009).

By the bimodal molecular mass distribution (MMD) (Fig. 2.3), the final properties of the material can be specifically influenced. The bimodal MMD is achieved by the specific incorporation of comonomers in several reactors. The short linear chains (low molecular weight) can be arranged in lamellar crystals, whereas the high molecular weight sections with short chain branches support the formation of tie-molecules and interlamellar entanglements. A higher number of tie-molecules and amorphous entanglements leads to a higher toughness and elongation at break of the material. This combination gives the material processability with good mechanical properties, which is important for long-term application.

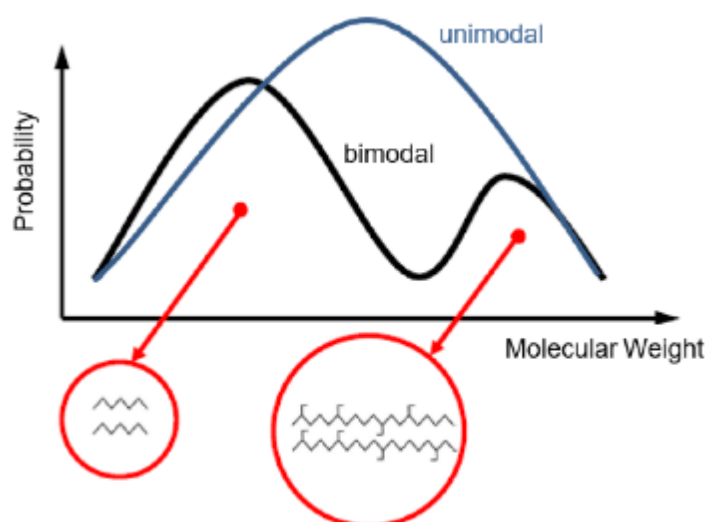


**Fig. 2.3:** Schematic representation of a unimodal and a bimodal MMD and the molecular structure of PE (Redhead, 2009).

The advantages of high-molecular and low-molecular PE can be exploited. Compared to other polymers, PE generally has a low density, low affinity to water adsorption, high chemical resistance, good processability as well as high toughness and elongation at break (Table 2.1) (Domininghaus et al., 2012).

**Table 2.1:** Properties of PA12 and HDPE.

Properties	PA12	HDPE
Density [kg/m <sup>3</sup> ]	1010 - 1040	940 - 960
Melting point [°C]	160 - 175	130 - 135
Crystallinity [%]	20 - 50	60 - 80
Tensile Modulus [MPa]	1200 - 1600	800 - 1300
Tensile Strain at Break	270 - 300	>500
Tensile Stress at Yield [MPa]	45 - 60	20 - 30

## 2.2 Failure Behaviour of Pressurized Polymer Pipes

The typical failure behaviour of pressurized polymer pipes can be described by using internal pressure curves (Fig. 2.4). Pipes are subjected to internal pressure without any external third-party loads. This curve shows the failure time as a function of the comparative stress in the pipe wall. It should be noted that it is shown in a double-logarithmic diagram (ISO 9080). Depending on the level of the equivalent stress, three characteristic failure ranges occur. A polymer can have all of these ranges or only partial ranges of the creep rupture curve. This behaviour depends on

the polymer type, the loading conditions and also the temperature (Lang et al., 1997; Pinter, 1999; Haager, 2006).

- “Stage I”, ductile failure occurs with high equivalent stresses and short loading times. The fracture is mainly controlled by the yield stress and usually shaped like fish mouths. This failure is influenced by density, strength, temperatures and the type of polymer. The deformations or fractures usually occur at the smallest wall thicknesses or existing defects along the pipe.
- “Stage II”, with lower applied stresses and longer service times, quasi-brittle failure occurs, as can be seen from the change in the slope of the failure curve. Local inherent defects lead to crack initiation and slow crack growth with only small local plastic deformations at the crack front. This area is of particular importance for long-term application. To analyse the crack initiation and slow crack growth a standardized fracture mechanics method, called the cyclic cracked round bar (CRB) test, has been developed recently (Frank and Pinter, 2014; ISO 18489).
- “Stage III”, the failure time is independent of the applied stress. Due to aging and the resulting polymer degradation, here only brittle failure occurs.

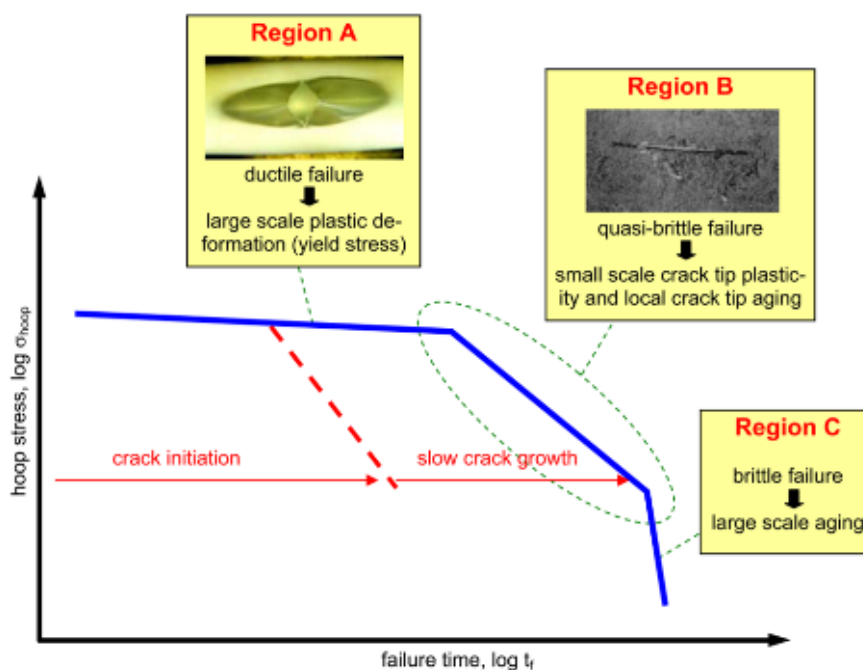


**Fig. 2.4:** Characteristic failure regions of pipes under internal pressure (Lang et al., 2005).

The HDPE types can be further divided according to ISO 9080. They are designated by the minimum required strength (MRS) in MPa after 50 years of operation in water and  $T = 23 \text{ }^\circ\text{C}$ . This means that PE80 or PE100 have an MRS of 8 or 10 MPa after 50 years (Brömstrup, 2009). The time-temperature dependent long-term hydrostatic strength  $\sigma_{\text{LTHS}}$  of a pipe is calculated with a standard extrapolation method according to ISO 9080 at a specific  $T$  and a life-time of 50 years. In the standard extrapolation method, the experimentally determined data, applied stress  $\sigma$  and time until failure  $t_f$  are plotted in a double-logarithmic  $\sigma$ - $t$  diagram. Afterwards the parameters  $k$  and  $d$  are determined by linear regression according to Eq. 2.1.

$$\log \sigma = -k \cdot \log t + d \quad (2.1)$$

For  $\sigma_{\text{LTHS}}$ ,  $\sigma$  at a life-time of 50 years ( $t = 50 \text{ years}$ ) is calculated using the previously evaluated parameters  $k$  and  $d$ . For a PE100 pipe grade,  $\sigma_{\text{LTHS}}$  at  $T = 23 \text{ }^\circ\text{C}$  must be higher than the MRS value of 10 MPa.

In frame of this thesis Stage I failure with dominating yielding processes is investigated. The molecular deformation processes of yielding are explained, followed by the Eyring theory and the kinetic fracture theory. During yielding the strain increases while the stress remains constant or drops down for the first time. The plastic flow processes start and an irreversible plastic deformation remains in the material, as the polymer chains slide off each other. Premature damage can occur before  $\sigma_y$  is reached, but this cannot be measured by a conventional tensile test (Grellmann and Seidler, 2011).

### 2.2.1 Deformation processes of yielding in semi-crystalline Polymers

There are two different molecular deformation processes contributing to the yield stress  $\sigma_y$  (Roetling, 1966; Hiss et al., 1999). In the diagram in Fig. 2.5,  $\sigma_y$  versus the strain rate  $\dot{\epsilon}$  at  $T = 65 \text{ }^\circ\text{C}$  of a PE is illustrated. The dependency of  $\sigma_y$  on  $\dot{\epsilon}$  is recognizable,  $\sigma_y$  increases with increasing  $\dot{\epsilon}$ . Two different slopes can be detected, which can be attributed to two different molecular deformation processes. The first slope is associated with intralamellar deformations at lower strain or stress rates ( $\dot{\epsilon}$  or  $\dot{\sigma}$ ) and lower  $T$  (process I). This kind of deformation is assigned to crystal slips within the crystals and lamellar fragmentation. In the second process (process II) the amorphous phase between the lamellar crystals is deforming. Stems are inside

different lamellar crystals and connected to tie-molecules through the amorphous phase. These stems have to be pulled through the crystals lattice while the lamellar crystals are kept intact (Bowden and Young, 1974). This interlamellar deformation contributes to  $\sigma_y$ . At low  $\dot{\epsilon}$ ,  $\dot{\sigma}$  or high  $T$ , the stems are able to move freely inside and outside the crystals leading to a negligible contribution of process II to  $\sigma_y$ . The deformation processes can be analysed by wide angle X-ray scattering (WAXS) measurements (Hiss et al., 1999).

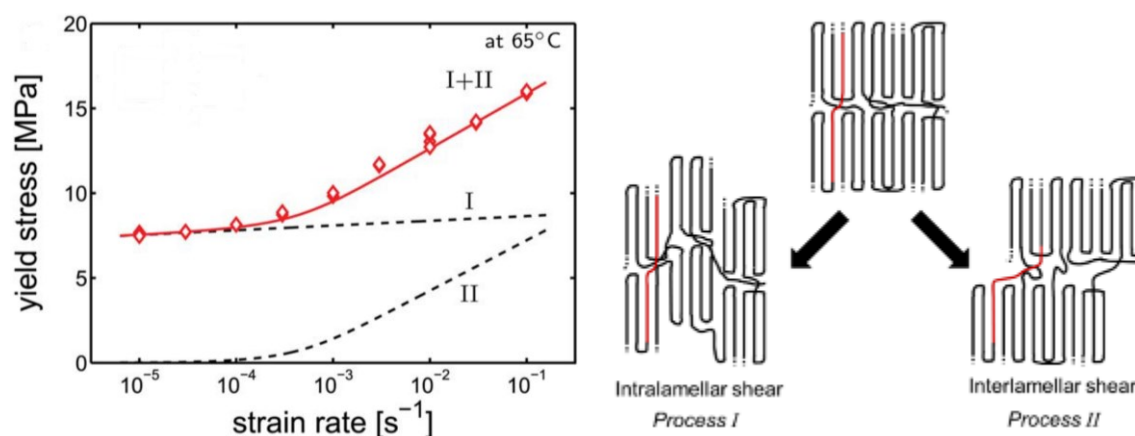


**Fig. 2.5:** Left: Illustration of  $\sigma_y$  versus  $\dot{\epsilon}$  at  $T = 65^\circ\text{C}$  and the contribution to  $\sigma_y$  of both processes. Right: Schematic representation of the two different molecular deformation processes (Pepels, 2015).

### 2.2.2 Eyring Theory

The Eyring theory describes activation energy dependent processes. In chemistry, the reaction and the reaction rate of the educts into the products via the transition state can be explained with this theory. By the Eyring theory of viscosity, the dependency of yielding on the loading rate  $\dot{\epsilon}$  and temperature  $T$  can be described. In general, the yield stress  $\sigma_y$  increases as  $\dot{\epsilon}$  increases or  $T$  decreases. In Fig. 2.6-left it is shown, that with increasing  $\dot{\epsilon}$  the strain at break  $\epsilon_b$  decreases and the yield stress  $\sigma_y$  increases. Further in Fig. 2.6-right, that  $\epsilon_b$  increases and  $\sigma_y$  decreases with increasing  $T$ . The resulting failure behaviour changes by varying  $\dot{\epsilon}$  and can be extrapolated. The Eyring theory assumes a process in which an energy barrier, activated thermally or additionally by applied stresses  $\sigma$ , must be overcome. Once the energy barrier is overcome, changes of polymer chain and chain segment localities occur. The accumulation of the local changes lead to an irreversible



deformation process. The additionally  $\sigma$  causes a reduction of the height of the barrier, enhancing the possibility for local changes.

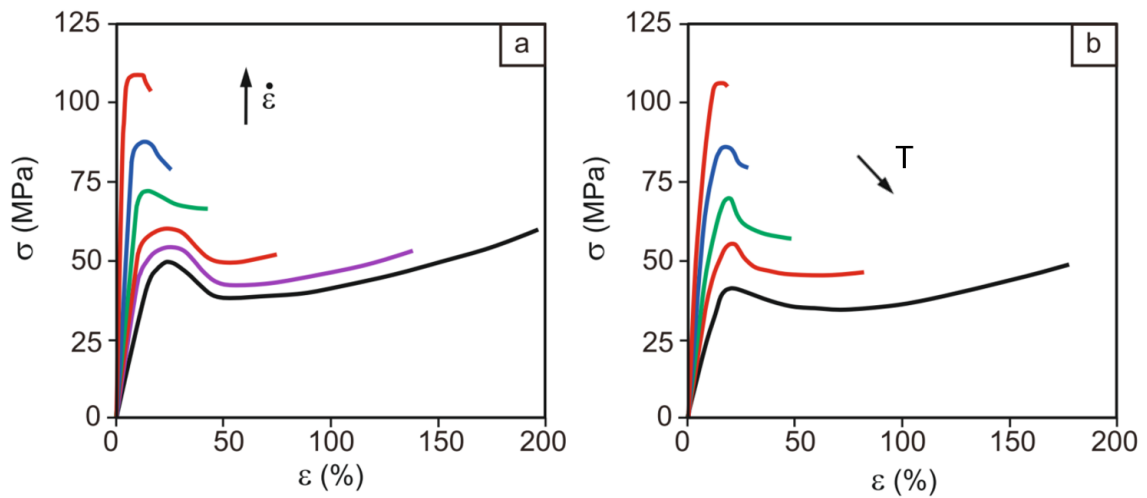


**Fig. 2.6:** Schematic  $\sigma$ - $\varepsilon$  diagram of a thermoplastic material as a function of the loading rate  $\dot{\varepsilon}$  (left) and the temperature  $T$  (right) (Grellmann and Seidler, 2011).

It is assumed that the macroscopic strain rate  $\dot{\varepsilon}$  is proportional to the rate of local changes. Thus, at high stresses where yielding is dominant, the Eyring theory can be used to describe the relationship between  $\dot{\varepsilon}$  and the applied stress  $\sigma$  (Eq. 2.2). By transforming Eq. 2.2 to  $\frac{\sigma}{T}$  (Eq. 2.3), the dependence of  $\sigma_y$  on  $\dot{\varepsilon}$  and  $T$  can be shown (Fig. 2.7). It should be noted, that in the diagram only  $\dot{\varepsilon}$  is plotted logarithmically. It can be seen that the dependence follows a linear correlation (Eyring, 1936; Kinloch and Young, 1995; Bauwens-Crowet et al., 1974).

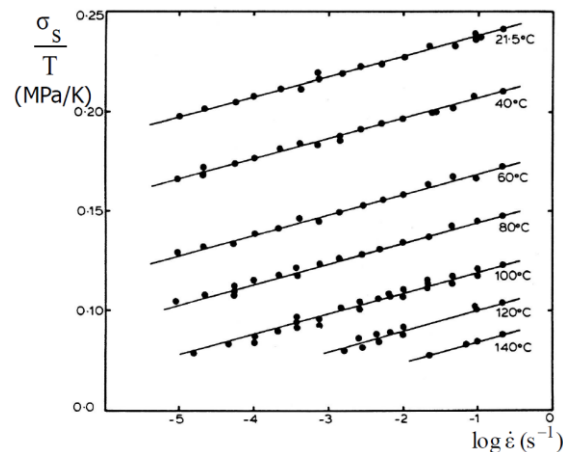


**Fig. 2.7:** Ratio of  $\frac{\sigma}{T}$  against the logarithm of  $\dot{\varepsilon}$  (Bauwens-Crowet et al., 1974).

$$\dot{\epsilon} = A \cdot e^{-\frac{\Delta E^* - v^* |\sigma|}{R \cdot T}} \quad (2.2)$$

$$\frac{\sigma}{T} = \frac{\Delta E^*}{v^* \cdot T} + \frac{R}{v^*} \ln \frac{\dot{\epsilon}}{A} \quad (2.3)$$

with:

$\dot{\epsilon}$  strain rate [ $s^{-1}$ ]

$A$  constant [ $s^{-1}$ ]

$\Delta E^*$  energy barrier [J]

$v^*$  activation volume [ $m^3$ ]

$\sigma$  applied stress [MPa]

$R$  universal gas constant [8.31451 J/mol\*K]

$T$  temperature [K]

A mathematical description of aforementioned deformation processes at yielding can be gained by a Ree-Eyring modification of the Eyring theory (Eq. 2.4). Both processes act independently, so their stress contributions can be added (van Erp et al., 2012; Klompen and Govaert, 1999; Bauwens et al., 1969; Pepels, 2015; Ree and Eyring, 1955).

$$\sigma_y(\dot{\epsilon}, T) = \sum_{i=I, II} \frac{k \cdot T}{V_i} \cdot \sinh^{-1} \left[ \frac{\dot{\epsilon}}{\dot{\epsilon}_{0,i}} \cdot e^{\frac{\Delta U_i}{R \cdot T}} \right] \quad (2.4)$$

with:

$\sigma_y$  yield stress [MPa]

$k$  Boltzmann's constant [ $1.381 \cdot 10^{-23}$  J/K]

$R$  universal gas constant [8.31451 J/mol\*K]

$T$  temperature [K]

$V_i$  activation volume [ $m^3$ ]

$\Delta U_i$  molar activation energy [J/mol]

$\dot{\epsilon}_{0,i}$  pre-exponential (fit) factor of each of the two processes  $i$  [ $s^{-1}$ ]

$\dot{\epsilon}$  applied strain rate [ $s^{-1}$ ]

### 2.2.3 Kinetic Fracture Theory

In kinetic fracture theory, a bond rupture is assumed to be a basic fracture event. In Fig. 2.8, state A are intact bonds and state B are broken bonds. The accumulation of individual bond fractures ultimately leads to total failure of the specimen. A breaking of bonds only occurs, if the free energy difference  $\Delta G_f$  is increased (Fig. 2.8 a). In the unloaded conditions a body is stable, by applying stress the ground level changes. The free energy change  $\Delta G_f$  becomes negative, when the applied stress  $\sigma_c$  is at a sufficiently high level (Fig. 2.8-b). The activation energy barrier  $\Delta G_{AB}^*$  for chain splitting is lowered by  $\sigma_c$  and the reaction of bond breaking is preferred. If  $\Delta G_f$  is negative, state B (bond breaking) is more likely. The bond breakage rate is controlled by  $\Delta G_{AB}^*$  (Bueche, 1957, 1958; Halpin, 1964; Halpin and Bueche, 1964; Zhurkov, 1965; Zhurkov and Tomashevsky, 1966). By measuring the time until failure  $t_f$  (Eq. 2.5) of specimens held under an applied constant stress  $\sigma_c$  the theory can be tested. This theory can also be applied to other molecular mechanisms, such as sliding of polymer chains. Here state A would describe intact chains and state B would be chains, which are slipped off against each other (Kinloch and Young, 1995).

$$t_f = t_0 \cdot e^{\frac{(\Delta G^* - v^* \sigma_c)}{R \cdot T}} \quad (2.5)$$

with:

$t_f$	time until failure [s]
$t_0$	reciprocal of the molecular oscillation frequency [s]
$\Delta G^*$	molar activation energy [J/mol]
$v^*$	molar activation volume [m <sup>3</sup> /mol]
$R$	universal gas constant [8.31451 J/mol*K]
$T$	temperature [K]
$\sigma_c$	constant stress [MPa]

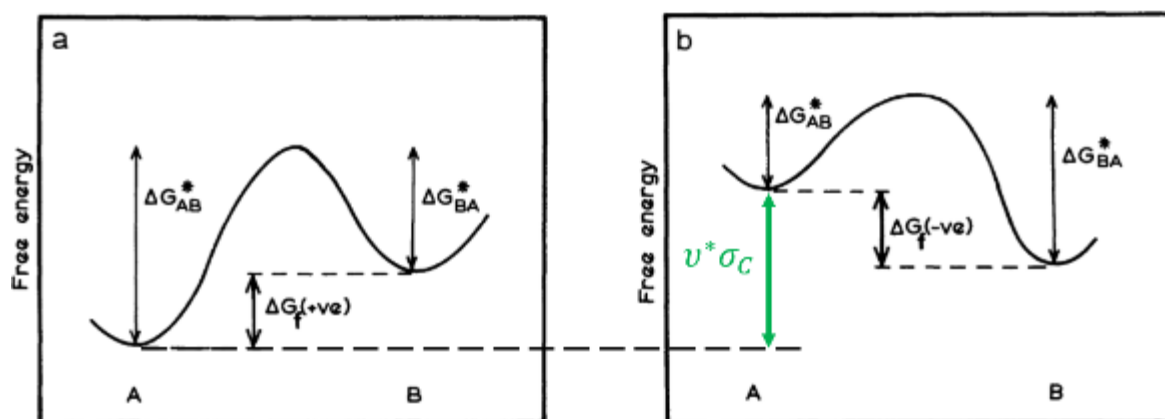


**Fig. 2.8:** Schematic representation of the free energy change  $\Delta G_f$ , for bond rupture, where state A are intact bonds and state B broken bonds. a) no applied stress ( $\Delta G_f$  increases) and b) applied stress  $\sigma_c$  ( $\Delta G_f$  decreases) (Kinloch and Young, 1995).

### 2.3 Accelerated Methods for long-term Failure Prediction

This chapter provides a brief overview of two different accelerated methods. These are the Stress-Rate accelerated Creep Rupture (SRCR) test (Gloggnitzer et al., 2018) and the accelerated screening method of long-term plasticity-controlled failure of pipe grades (Kanters et al., 2016), which shall be termed “K-test” in the following. Both methods are capable of predicting material lifetimes under static loading conditions. The SRCR-test is controlled by stress and the K-test by strain. However, the K-test is based on a Ree-Eyring modification of the Eyring theory and was developed for characterizing the ductile failure behaviour of polymer pipes (Stage I failure), whereas the SRCR-test is an approach to predict the life-time of composites and is not based on a failure theory. To determine only the critical stress, where the unusual ductile-brittle transition occur, there are two different methods. These methods only identify the critical stresses and do not provide any information about time until failure. The first method is the strain rate ( $\dot{\epsilon}$ ) dependent Delayed Necking Test (Zhou et al., 1999; Zhou et al., 2005) and the second is a multi-relaxation test, also called D-Split Test (Tan and Jar, 2019; Jar, 2019). They are not further described in the following chapter, as they only provide the critical stress and no long-term behaviour.

### 2.3.1 SRCR-Test

This test method was developed for brittle composite materials to predict material strength over the whole lifetime. It is a method based on phenomenological approaches. For the mechanical long-term characterization, modified creep rupture tests were performed. First of all, ISO 527 tensile tests are carried out to get a first overview of the mechanical properties of the material. In doing so, the specific reference stress level  $\sigma_{\text{ref}}$  can be determined in relation to the tensile stress at break  $\sigma_b$ . The normalized stress levels are chosen between  $65\% < \sigma_N < 100\%$  and is calculated according to Eq. 2.6.

$$\sigma_N = \frac{\sigma}{\sigma_b} \quad (2.6)$$

At the beginning of this method, materials are loaded to a specific stress level ( $\sigma_{\text{ref}}$ ) followed by a constant stress rate ( $\dot{\sigma}$ ) until total failure. The loading conditions are illustrated in Fig. 2.9-left. By changing  $\dot{\sigma}$  in various tests, the rupture time at a stress rate of zero can be determined by extrapolation, which is comparable to a classic creep rupture test (static loading conditions) at  $\sigma_{\text{ref}}$ . The tests give the stress rate-dependent failure strength with the corresponding time to failure  $t_f$ . That procedure is performed repeatedly at different  $\sigma_{\text{ref}}$  to predict  $t_f$  under static loading conditions. By plotting all  $\sigma_{\text{ref}}$  and the predicted  $t_f$  in one diagram, the long-term material performance can be described (Fig. 2.9-right). It should be noted, that the overall testing time for brittle materials is less than a week and therefore significantly faster than classic creep rupture tests (Gloggnitzer et al., 2018).

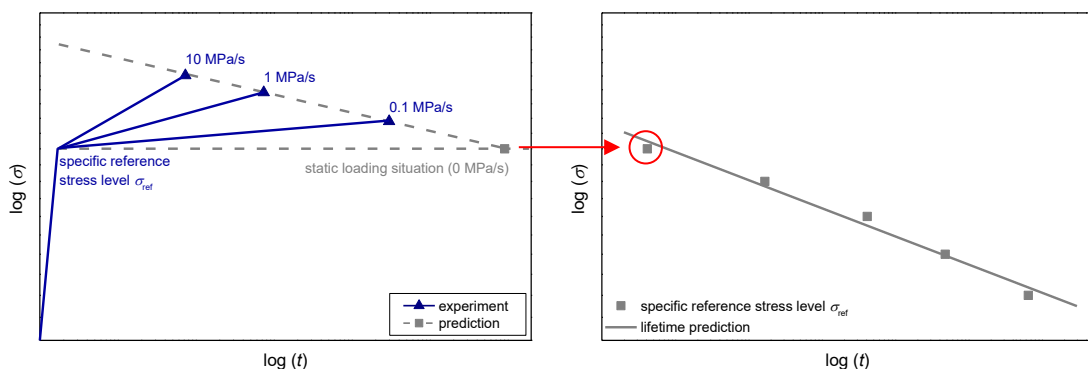


**Fig. 2.9:** Schematic illustration of the loading conditions of the SRCR-test on the left side and the lifetime prediction on the right side (Gloggnitzer et al., 2018).

### 2.3.2 Accelerated long-term plasticity-controlled test

The concept of this method is to perform three different tests (tensile, creep and compression) to evaluate long-term plasticity-controlled failure. First, tensile tests at different  $\dot{\epsilon}$  and  $T$  are done to determine  $\dot{\epsilon}$  and  $T$  dependency of  $\sigma_y$ . By performing compression tests, the compression yield stress  $\sigma_c$  is measured. In Fig. 2.10-left, the dependence of the engineering  $\sigma_y$  and  $\sigma_c$  on  $\dot{\epsilon}$  and  $T$  is illustrated. It shows, that at higher  $T$  no linear correlation for  $\sigma_y$  and  $\dot{\epsilon}$  exists any more (chapter 2.2.1). According to Eq. 2.7, the pressure dependence term  $\mu$  can be calculated with  $\sigma_c$  and  $\sigma_y$  of the compression and tensile tests.

$$\mu = 3 \cdot \frac{\sigma_c - \sigma_y}{\sigma_c + \sigma_y} \quad (2.7)$$

with:

- $\mu$  pressure dependence term [-]
- $\sigma_c$  compression yield stress [MPa]
- $\sigma_y$  tensile yield stress [MPa]

By means of classic creep tests at stresses of the order of  $\sigma_y$  (Fig. 2.10-right), the critical strain  $\epsilon_{cr}$  and  $t_f$  is determined. In Fig. 2.10 the dependency of  $t_f$  on  $\sigma$  can be evaluated,  $t_f$  is additionally also influenced by the temperature. In comparison to  $t_f$ ,  $\epsilon_{cr}$  is not significantly influenced by  $T$  and  $\sigma$  independent, in the following a constant  $\epsilon_{cr}$  is assumed. Also, the plastic flow rate  $\dot{\epsilon}_{pl}$ , also dependent on  $\sigma$  and  $T$ , can be evaluated (Eq. 2.8). In this case  $\epsilon_{cr}$  is the strain that is achieved at  $\dot{\epsilon}_{pl}$  until failure occurs. The strain-time diagram of the classic creep test for a polycarbonate (PC) is shown in Fig. 2.10-right.

$$t_f = \frac{\epsilon_{cr}}{\dot{\epsilon}_{pl}} \quad (2.8)$$

with:

- $t_f$  time until failure [s]
- $\epsilon_{cr}$  critical strain [%]
- $\dot{\epsilon}_{pl}$  plastic flow rate [ $s^{-1}$ ]

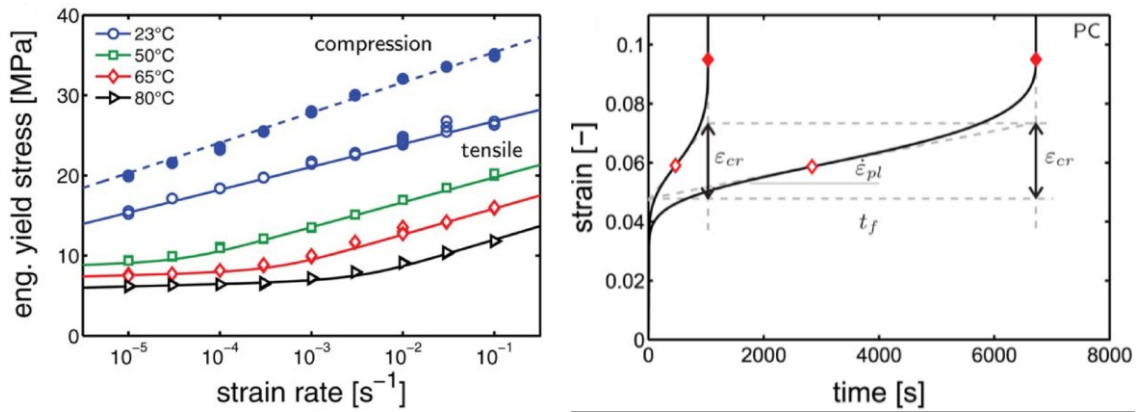


**Fig. 2.10:** Left: Illustration of the dependency of  $\sigma_y$  and  $\sigma_c$  on  $\dot{\epsilon}$  and  $T$  of PE, by performing tensile and compression tests at different  $\dot{\epsilon}$ . Right: Illustration of  $\epsilon_{cr}$ ,  $\dot{\epsilon}_{pl}$  and  $t_f$  for PC at high and low applied  $\sigma$ , by performing classic creep tests (Kanters et al., 2016).

Applying the Ree-Eyring modification of the Eyring theory, for both independently acting deformation processes of yielding (chapter 2.2.1, Eq. 2.9), a model for life-time prediction can be created by introducing the pressure term  $\mu * p$  (Eq. 2.10). The hydrostatic pressure  $p$  is identical for both, in chapter 2.2.1 mentioned processes, that contribute yielding and is multiplied by the pressure dependence term ( $\mu$ ). Each process has its own activation energy  $\Delta U_i$ , activation volume  $V_i$ , and pre-exponential (fit) factor  $\dot{\epsilon}_{0,i}$ . The formula for the consideration of pressure dependency is as follows:

$$\sigma(\dot{\epsilon}_{pl}, T) = \sigma_I(\dot{\epsilon}_{pl}, T) + \sigma_{II}(\dot{\epsilon}_{pl}, T) \quad (2.9)$$

$$= \sum_{i=I, II} \frac{k \cdot T}{V_i} \cdot \sinh^{-1} \left[ \frac{\dot{\epsilon}_{pl}}{\dot{\epsilon}_{0,i}} \cdot e^{\frac{\Delta U_i}{R \cdot T}} \right] + \mu \cdot p \quad (2.10)$$

Experimental data points are fitted with the model and the material constants  $V_i$ ,  $\Delta U_i$ ,  $\dot{\epsilon}_{0,i}$  are evaluated for each deformation process. Combining the Ree-Eyring model and the material constant  $\epsilon_{cr}$ , a prediction of  $t_f$  at a certain  $\sigma$  can be made, by extrapolation of the model to lower stress levels. These tests were successfully performed on PC and PE (Kanters, 2015), as can be shown in Fig. 2.11. In the diagram the experimental data and the model calculated with the Ree-Eyring modification are illustrated and the material behaviour is shown.

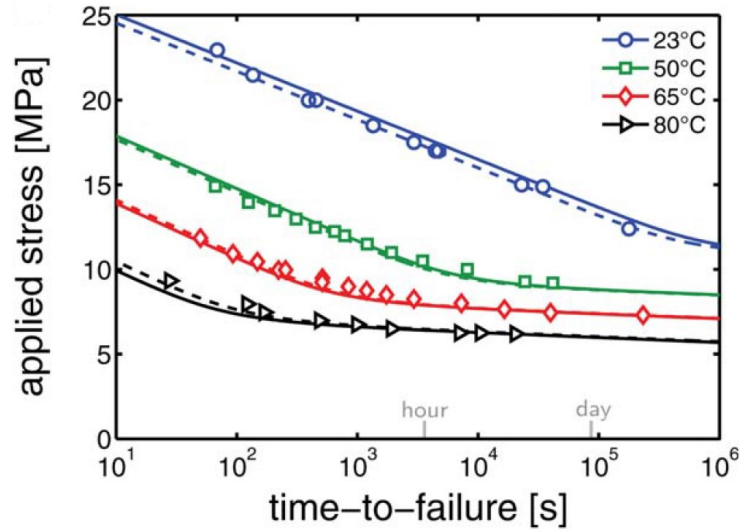


**Fig. 2.11:** The experimental data (markers) and the model (lines) using Eq. 2.9 at different  $T$  for PE (Kanters et al., 2016).

The model can be extrapolated to lower applied stresses  $\sigma$  and a prediction of  $t_f$  can be conducted. The testing time of this method for one material is about two weeks.

## 2.4 Equivalent stress hypotheses

Most of the accelerated methods are based on uniaxial tests. However, multiaxial stress states occur in pipes. In order to compare a uniaxial stress state with a multiaxial stress state, the latter must first be converted into an equivalent stress. In the following, two hypotheses are discussed in detail.

For a thin-walled pipe the occurring stresses can be determined using the Barlow's formula (Eq. 2.11 - 2.13). For the hypotheses,  $\sigma_1$  corresponds to the hoop stress  $\sigma_h$ ,  $\sigma_2$  to the axial stresses  $\sigma_a$  and  $\sigma_3$  to the radial stresses  $\sigma_r$ , which can be neglected compared to  $\sigma_h$  and  $\sigma_a$  ( $\sigma_r = \sigma_3 = 0$ ) (Böge and Böge, 2017; Visser et al., 2010; Kanters et al., 2016).

$$\sigma_h = \frac{p \cdot d_m}{2 \cdot s} \quad (2.11)$$

$$\sigma_a = \frac{p \cdot d_m}{4 \cdot s} \quad (2.12)$$

$$\sigma_r = -\frac{p}{2} \quad (2.13)$$



with:

$p$	internal pressure [bar]
$d$	inner diameter [m]
$s$	wall thickness [m]
$d_m$	mean diameter $d_m = d + s$ [m]

#### 2.4.1 Maximum stress criterion according to von Mises

In this criterion, failure of the component occurs, if the shape modification energy exceeds a limit value. It is used for tough materials under static and dynamic loads. For the calculation of the equivalent stress  $\sigma_{VM}$ , Eq. 2.14 is used. By setting  $\sigma_r$  to zero and substituting  $\sigma_a$  with  $\frac{\sigma_h}{2}$ , a factor of  $\frac{\sqrt{3}}{2}$  is obtained (Böge and Böge, 2017; Visser et al., 2010; Kanters et al., 2016).

$$\sigma_{VM} = \sqrt{\frac{1}{2} [(\sigma_h - \sigma_a)^2 + (\sigma_a - \sigma_r)^2 + (\sigma_r - \sigma_h)^2]} \rightarrow \sigma_{VM} = \frac{\sqrt{3}}{2} \sigma_h \quad (2.14)$$

#### 2.4.2 Maximum shear criterion according to Tresca

According to Tresca, the highest principal stress difference is responsible for the failure of the material. This difference corresponds to twice the value of the maximum shear stress. It is therefore applied to tough materials under static loads, which fail by yielding. In a multiaxial stress state, the equivalent stress is calculated using Eq. 2.15 (Böge and Böge, 2017; Visser et al., 2010; Kanters et al., 2016).

$$\sigma_T = \max (|\sigma_h - \sigma_a|; |\sigma_a - \sigma_r|; |\sigma_r - \sigma_h|) \rightarrow \sigma_T = \sigma_h \quad (2.15)$$

### 3 EXPERIMENTAL

At the beginning of this section the specific materials and the available test specimens used in this thesis and the relevant basic methods for material characterization are discussed. Then the modified method based on the SRCR-test and the evaluation are explained.

#### 3.1 Materials

The modification of the SRCR-test (mSRCR) was accomplished with the aid of four different commercially available pipe grade materials - a PA12 (MRS = 18 MPa) which is used in gas applications and three PE100 (MRS = 10 MPa) (termed PE1, PE2 and PE3 in the following), which are used in water distribution systems. The materials were available in the form of ISO 527-2 multipurpose test specimens type B. The specimens of PE1, PE2 and PE3 were produced by an external manufacturer not like PA12, which was produced by the material manufacturer. For the determination of the density, melt flow rate (MFR) and thermal properties via differential scanning calorimetry (DSC) the virgin granulate was used, therefore no sample preparation was necessary.

#### 3.2 Basic Material Characterization

This chapter briefly explains the determination of the general material characteristics and the parameters used. The physical, rheological, thermal and mechanical data were determined.

##### 3.2.1 Density

The density was measured according to ISO 1183 using the Archimedes' principle. An analytical balance type AG 204 Deltarange (Mettler Toledo GmbH, Schwerzenbach, Switzerland) and distilled water without additional wetting agent as auxiliary liquid were used for this purpose. Three measurements of each material were performed at a  $T = 24.1$  °C. The weight of the granulate of the different measurements was between  $m = 1.5 - 2$  g.

### 3.2.2 Melt Flow Rate

The MFR was determined on an MF20 (CEAST, Torino, Italy) melt index tester. The measurements were carried out at  $T = 190\text{ }^{\circ}\text{C}$  and a load of 5 kg in according ISO 1133. For each measurement and material, four strings were cut off and weighted in 10 minutes intervals.

### 3.2.3 Differential Scanning Calorimetry

A DSC6000 apparatus (Perkin Elmer Instruments, Waltham, USA) was used to perform the measurements. The calibration of the temperature scale was performed by the melting characteristics of Indium and Zinc. The measurements were taken according to ISO 11357 in an aluminium pan with Nitrogen as purge gas (50.0 ml/min). Two heating processes and one cooling process for each material with a heating and cooling rate of 10 K/min were performed, whereby the temperature was kept constant for 5 min at the beginning and the end of each heating and cooling process. The measuring range for PA12 was  $0\text{ }^{\circ}\text{C} \leq T \leq 230\text{ }^{\circ}\text{C}$  and  $25\text{ }^{\circ}\text{C} \leq T \leq 200\text{ }^{\circ}\text{C}$  for PE1, PE2 and PE3. The sample weight for PA12 was  $m = 3.150\text{ mg}$ ,  $m = 11.00\text{ mg}$  for PE1,  $m = 11.36\text{ mg}$  for PE2 and  $m = 11.18\text{ mg}$  for PE3. Only one measurement was performed to get an overview of the melting behaviour and to calculate the crystallinity of the material. Evaluation was carried out with the associated software Pyris™. In Fig. 3.1 the heat flux  $\dot{Q}$  over the temperature  $T$ , with the determined material parameters is illustrated. For the determination of the material parameters (Fig. 3.1), the heat of fusion  $\Delta H_m$ , melting temperature  $T_m$  and the degree of crystallization  $D$  the second heating process was used. During the second heating the thermal history, that influences the previously mentioned parameters, is no longer visible. The degree of crystallization  $D$  as given in Eq. 3.1, is the ratio between  $\Delta H_m$  and its equilibrium melting enthalpy  $\Delta H_m^0$  (melting enthalpy of a theoretically 100 % crystalline material). The equilibrium melting enthalpy  $\Delta H_m^0$  of a theoretically 100 % crystalline material is found to be  $\Delta H_m^0 = 245\text{ J/g}$  and  $\Delta H_m^0 = 293\text{ J/g}$  for PA12 and PE, respectively (Wunderlich, 2005).

$$D = \frac{\Delta H_m}{\Delta H_m^0} \cdot 100 \quad (3.1)$$

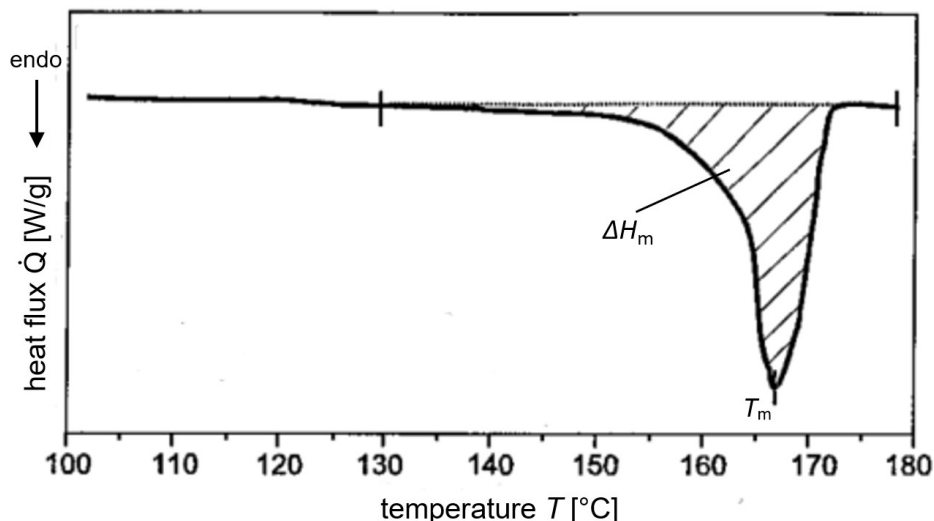


**Fig. 3.1:** Schematic representation of a heating process, with the material parameters  $T_m$  and  $\Delta H_m$  (Ehrenstein et al., 2003).

### 3.2.4 Tensile Tests

The tensile properties of the materials are determined according to ISO 527. Five specimens of each material were measured and evaluated. The measurements were performed on a tensile/compression-universal testing machine type Z010 (ZWICK GmbH & Co. KG, Ulm, Germany) with a 10 kN load cell at  $T = 23$  °C and 80 °C. The measurements and the specimens conditioning at  $T = 80$  °C with an accuracy of  $\pm 1$  °C are performed in a temperature chamber. The determination of the tensile modulus  $E$  is carried out at a test speed of 1 mm/min. Subsequently, measurements are performed until failure at a test speed of 50 mm/min. Until the yield stress is reached, the elongation is measured by external extensometer, then via the crosshead of the machine.

### 3.3 Modification of the SRCR-Test

When the loading rate  $\dot{\epsilon}$  increases during a uniaxial tensile test of polymers, an increase in the yield stress  $\sigma_y$  is to be expected due to the plastic effect described by the Eyring theory (compare chapter 2.2.2, Fig. 2.6-left) and can be extrapolated due to the dependency. A similar phenomenon can be observed when the temperature  $T$  is increased, as shown in Fig. 2.6-right, when  $T$  is increased,  $\sigma_y$  decreases.

The SRCR-test is designed for brittle materials such as composites (Gloggnitzer et al., 2018). The failure mechanism of brittle materials and tough materials are different. The SRCR-test applied within this thesis is based on phenomenological approaches, and rely on the correlations that  $\sigma_y$  increases when  $\dot{\epsilon}$  increases, or  $T$  decreases, respectively. If the correlation is given, an extension of the method to tough materials is possible. The specimen is first loaded with a specific reference stress level  $\sigma_{ref}$ . Then this load is continuously increased with a defined stress rate  $\dot{\sigma}$  until total failure occurs. This test will be repeated several times for the same  $\sigma_{ref}$  but with changing  $\dot{\sigma}$ . Despite the preloading  $\sigma_{ref}$ , the dependence of the deformation and failure behaviour of the specimen on the loading rate is expected. In this master thesis, it will be investigated whether the dependency is still given with this modified SRCR-test (mSRCR) procedure. If the deformation behaviour of the materials in this test show a clear dependency on the stress rate, an extrapolation of the failure behaviour will be carried out. The dependency is given, if a correlation can be determined by plotting  $\sigma_y$  against the loading rate, as can be seen in chapter 2.2.2 in Fig. 2.7. In the mSRCR-test the loading rate is controlled by stress, therefore it will be termed  $\dot{\sigma}$  in the following. Subsequently, the test is carried out at higher  $T$ , to analyse also this influence on  $\sigma_y$  too.

For the modification of the method (mSRCR), first of all the specific reference stresses  $\sigma_{ref}$  and stress rates  $\dot{\sigma}$  for each material were considered. Different  $\sigma_{ref}$  were selected based on the available results of the ISO 9080 measurements for these materials, especially the applied stresses were used to define  $\sigma_{ref}$  in a similar range. For extrapolation, measurements must be carried out at different loading rates, i.e.  $\dot{\sigma}$  of 1, 0.1, 0.01, 0.005 and 0.001 MPa/s. The load rate should be in the same range so that the failure behaviour keeps identical for all measurements.

All measurements were performed on a tensile/compression-universal testing machine type Z010 (ZWICK GmbH & Co. KG, Ulm, Germany) with a 10 kN load cell at  $T = 23\text{ }^{\circ}\text{C}$  and  $80\text{ }^{\circ}\text{C}$  for both materials (PA12 and PE). Specimens were conditioned at the respective test temperature in a temperature chamber for 1 h before attaching them to the clamping unit and loading until  $\sigma_{ref}$  was reached. Subsequently, the specimens were loaded with different  $\dot{\sigma}$  and the time measurement started until total failure.

The following **Fehler! Verweisquelle konnte nicht gefunden werden.** summarizes  $\sigma_{\text{ref}}$  and  $T$  of the respective measurements. For each parameter three measurements were carried out, except for the measurements with  $\dot{\sigma}$  of 0.005 MPa/s and 0.001 MPa/s. For these parameters only two measurements were performed due to the higher time expenditure.

**Table 3.1:** Summary of the different parameters  $\sigma_{\text{ref}}$  and  $T$  of the mSRCR measurements for PA12, PE1, PE2 and PE3.

	$T$ [°C]	$\sigma_{\text{ref}}$ [MPa]
PA12	23	22 / 24 / 26 / 28 / 30
	80	12 / 13 / 14 / 15
PE1	23	11.5 / 12 / 12.5 / 13 / 13.5
	80	5 / 5.25 / 5.5 / 5.75 / 6
PE2	23	12 / 13 / 14 / 15
	80	5 / 6 / 7 / 8
PE3	23	11 / 12 / 13 / 14
	80	5 / 6 / 7 / 8

For the evaluation of this method, a conservative approach has been chosen, considering yielding as critical material parameter rather than rupture of the specimen. Due to the toughness of the non-reinforced materials, mean values of the stress rate-dependent yield stress  $\sigma_{y, \text{mSRCR}}$  and the corresponding time until yielding  $t_{y, \text{mSRCR}}$  were used for evaluation. The determination of  $\sigma_{y, \text{mSRCR}}$  and  $t_{y, \text{mSRCR}}$  is shown in Fig. 3.2. In both diagrams in Fig. 3.2  $\sigma_{y, \text{mSRCR}}$  is visible, but in the  $\sigma$ - $\varepsilon$  diagram of the test (Fig. 3.2-a) it is easier to determine  $\sigma_{y, \text{mSRCR}}$ . The parameters are detected as follows. First,  $\sigma_{y, \text{mSRCR}}$  is evaluated in the  $\sigma$ - $\varepsilon$  diagram of the test (Fig. 3.2-a), then  $t_{y, \text{mSRCR}}$  is read off in the  $\sigma$ - $t$  diagram (Fig. 3.2-b). For all individual measurements at different  $\sigma_{\text{ref}}$  and  $\dot{\sigma}$ ,  $\sigma_{y, \text{mSRCR}}$  and  $t_{y, \text{mSRCR}}$  are determined.

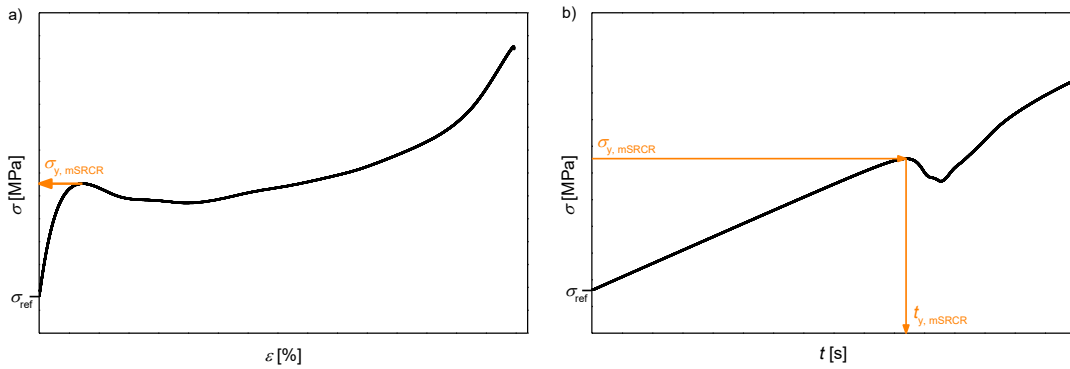


**Fig. 3.2:** Schematic diagram of a measurement a)  $\sigma$ - $\varepsilon$  diagram to determine  $\sigma_{y, mSRCR}$  and b)  $\sigma$ - $t$  diagram to determine  $t_{y, mSRCR}$ .

The modified evaluation approach for the mSRCR-test is schematically presented in Fig. 3.3. The mean values of the  $\sigma_{y, mSRCR}$  and  $t_{y, mSRCR}$  at the respective  $\dot{\sigma}$  are plotted in a double-logarithmic  $\sigma$ - $t$  diagram for each  $\sigma_{ref}$  and extrapolated to a static load level of  $\sigma_{ref}$ , which corresponds to the time until failure. For the mSRCR-test the time until yielding of a static load situation.

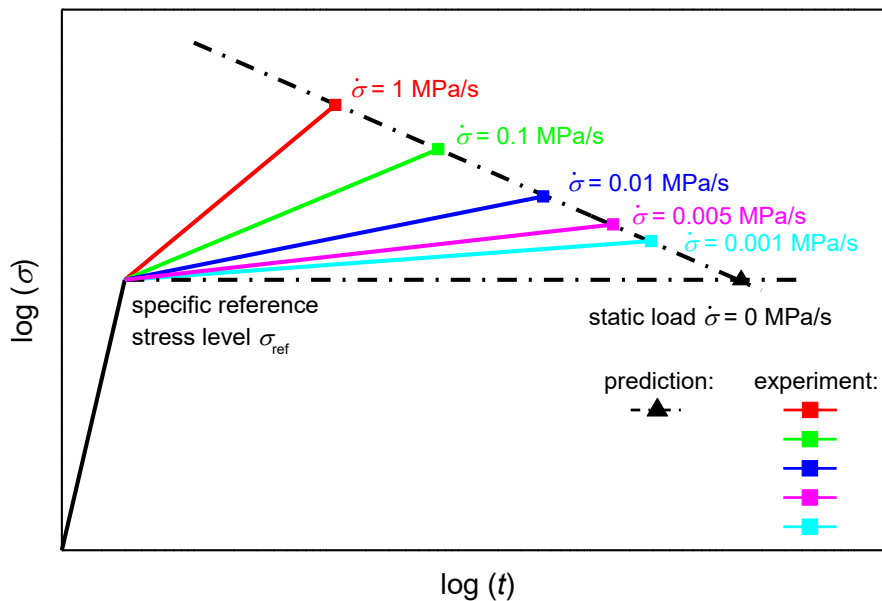


**Fig. 3.3:** Schematic representation of mSRCR-test at different  $\dot{\sigma}$  and extrapolation to static load  $\dot{\sigma} = 0$  MPa/s.

The measurements are then conducted at different  $\sigma_{ref}$ . Afterwards, all  $\sigma_{ref}$  and extrapolated  $t_f$  under  $\dot{\sigma} = 0$  MPa/s conditions are plotted in one diagram. This diagram represents the predicted long-term strength behaviour of multipurpose

specimens for the investigated material (Fig. 3.4). It is the result of the measurements at different  $\dot{\sigma}$  and extrapolation to a static load at  $\sigma_{\text{ref}}$ .

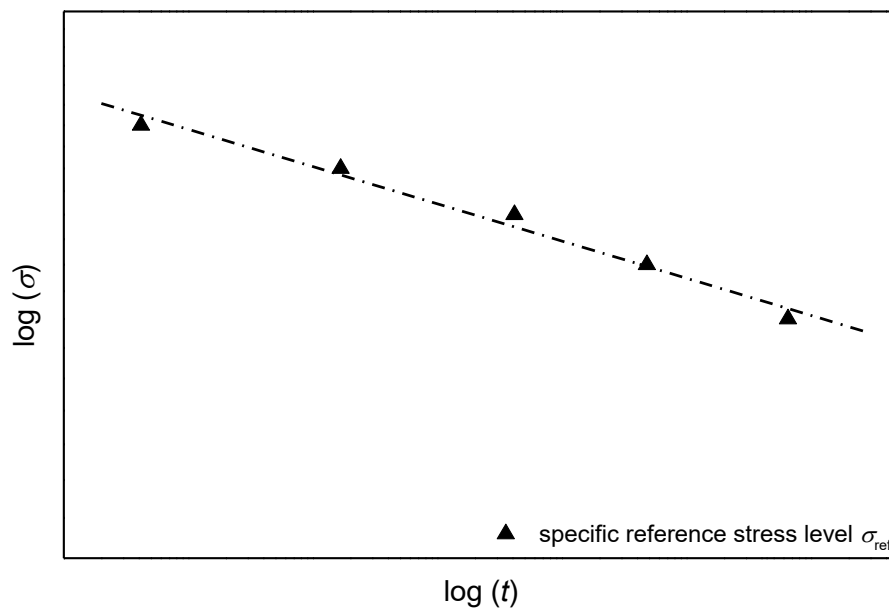


**Fig. 3.4:** Schematic illustration of the evaluation of the long-term strength behaviour.



## 4 RESULTS AND DISCUSSION

First, the results of the basic characterization techniques are discussed to get a first overview of the materials. The second part covers the application of the mSRCR test and the determination of Stage I failure curves for four different materials. The focus is put on the obtained knowledge of this method and its influencing factors. Furthermore, it is investigated and discussed whether the SRCR-test can be applied to tough materials and an extrapolation is possible to predict the long-term strength. Possible improvements for further development are considered. Finally, the Stage I failure curves determined via the mSRCR-test are compared to the ISO 9080 results of the respective materials.

### 4.1 Basic Material Properties

General material properties, such as density, MFR, DSC and tensile test results and standard deviations are summarized in Table 4.1. Following the order in Table 4.1, the different results are described in greater detail.

**Table 4.1:** Result of density  $\rho$  (ISO 1183), MFR (ISO 1133), melting temperature  $T_m$ , heat of fusion  $\Delta H_m$ , degree of crystallinity  $D$  (ISO 11357), tensile modulus  $E$ , tensile strain at break  $\varepsilon_b$  and tensile stress at yield  $\sigma_y$  (ISO 527) for PA12, PE1, PE2 and PE3.

Properties	Parameters	PA12	PE1	PE2	PE3
$\rho$ [kg/m <sup>3</sup> ]	24.1 °C	1008 ± 0,6	954 ± 0.5	951 ± 0.6	956 ± 0.8
MFR [g/10min]	190 °C/5.0 kg	0.1944 ± 0.005	0.2040 ± 0.005	0.1656 ± 0.003	0.2046 ± 0.0013
$T_m$ [°C]	10 K/min	174	132	131	132
$\Delta H_m$ [J/g]	10 K/min	48	152	182	188
$D$ [%]	10 K/min	20	52	62	64
$E$ [MPa]	23 °C	1020 ± 24	912 ± 19	821 ± 15	942 ± 46
	80 °C	189 ± 11	189 ± 17	-	-
$\varepsilon_b$ [%]	23 °C	> 200	12 ± 1.4	24 ± 1.8	17 ± 0.7
	80 °C	> 230	33 ± 6	-	-
$\sigma_y$ [MPa]	23 °C	35.4 ± 0.9	28.9 ± 0.5	24.6 ± 0.1	27.6 ± 0.2
	80 °C	-	14.6 ± 0.9	-	-

These measurements are done to get a first overview of the material properties and whether they also correspond to data found in literature (Table 2.1). For PE2 and PE3 no tensile tests at  $T = 80\text{ °C}$  were performed, since the number of test specimens was limited.

#### 4.1.1 Density and Melt Flow Rate

The results of the density and MFR measurements are in accordance with values depicted in literature in Table 2.1. For PA12 the density at  $24.1\text{ °C}$  is  $1008 \pm 0.6\text{ kg/m}^3$  and for the different PE types between  $951\text{-}956\text{ kg/m}^3$ . Compared to literature the value of PA12 is slightly lower and the values of PE are in the right range. These deviations are very small and can be neglected. For PE1 the MFR is  $0.25\text{ g/10min}$  according to the data sheet, for the other materials this value is not given in the data sheet or literature. The deviations in the MFR measurement can have different causes:

- i. Polymer strands are cut off by hand with a stopwatch every 10 minutes. The strands were not always cut at exactly the same time.
- ii. If granulate in the cylinder is not sufficiently compressed, air can be trapped, which leads to bubbles in the strand.
- iii. MFR values can vary slightly from batch to batch.

#### 4.1.2 Differential Scanning Calorimetry

To determine  $T_m$ ,  $\Delta H_m$  and  $D$ , the second heating curve was used, the heat flux  $\dot{Q}$  over  $T$  is shown in Fig. 4.1 and Fig. 4.2 for PA12, PE1, PE2 and PE3. Due to many influencing variables such as heating rate, purge gas flow, reference substance, sample weight etc., deviations may occur. If the sample weight is too high, the melting can be uneven, which affects the melt peak and therefore the evaluated properties. The  $T_m$  of the materials are in a comparative range (Table 2.1), for PA12  $T_m = 174\text{ °C}$  (literature  $160\text{-}175\text{ °C}$ ), for PE1  $T_m = 132\text{ °C}$ , PE2  $T_m = 131\text{ °C}$  and PE3  $T_m = 132\text{ °C}$  (in literature for HDPE  $130\text{ °C} < T_m < 135\text{ °C}$ ). For  $\Delta H_m$  no reference values are given in literature or in the data sheets,  $\Delta H_m$  for PA12 is  $48\text{ J/g}$  and lower in comparison to PE1 ( $152\text{ J/g}$ ), PE2 ( $182\text{ J/g}$ ) and PE3 ( $188\text{ J/g}$ ). Crystallinity values were calculated as 20 % for PA12, 52 % for PE1, 62 % for PE2 and 64 % for PE3.

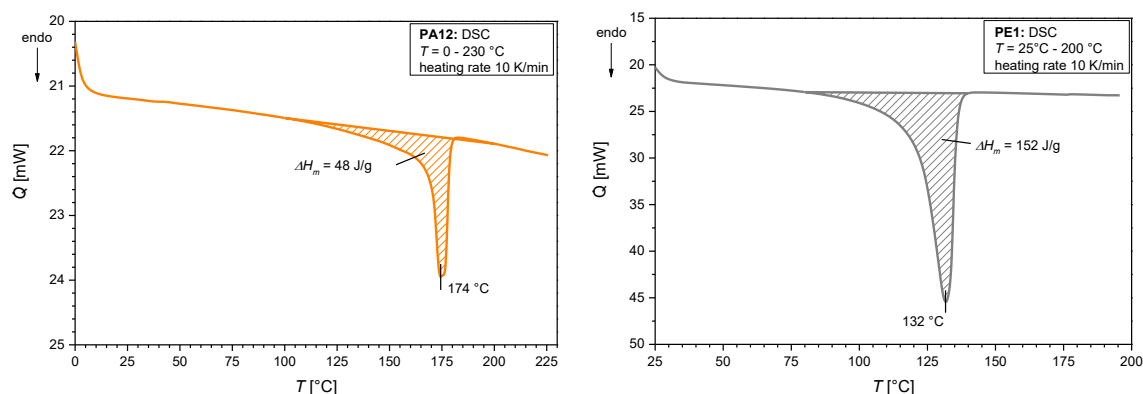


**Fig. 4.1:** The DSC melting curve progression from PA12 (left) and PE1 (right) at a temperature range of  $0 \text{ °C} \leq T \leq 230 \text{ °C}$  for PA12 and  $25 \text{ °C} \leq T \leq 200 \text{ °C}$  for PE1 and a heating rate of 10 K/min.

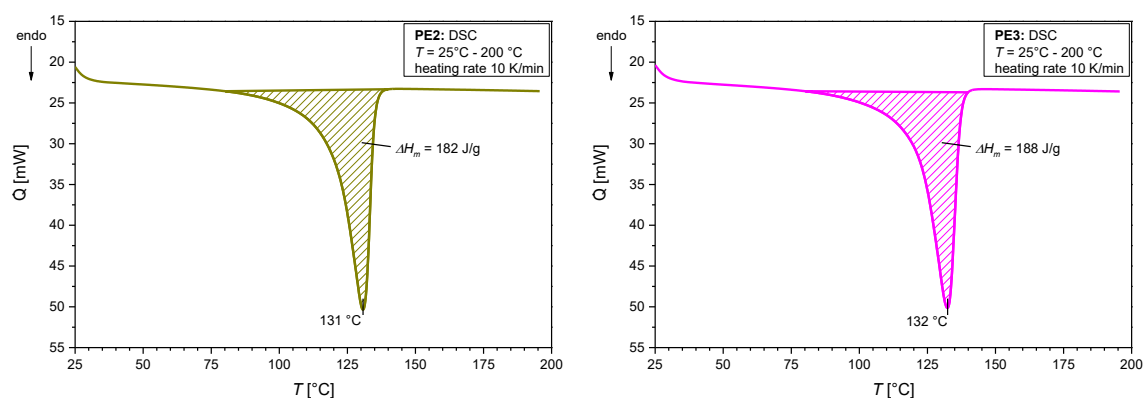


**Fig. 4.2:** The DSC melting curve progression from PE2 (left) and PE3 (right) at a temperature range of  $25 \text{ °C} \leq T \leq 200 \text{ °C}$  and a heating rate of 10 K/min.

#### 4.1.3 Tensile Tests

Representing tensile test results, Fig. 4.3 shows the graph for PA12 at  $T = 23 \text{ °C}$  (orange) and  $80 \text{ °C}$  (red). As expected a temperature increase, comes along with a decrease of  $E$  and  $\sigma_y$  as well as an increase of  $\epsilon_b$ . The values of  $E$  decrease from  $1020 \pm 24 \text{ MPa}$  to  $189 \pm 11 \text{ MPa}$ , whereas  $\epsilon_b$  increases from  $>200$  to  $>230 \%$ . At  $T = 80 \text{ °C}$ , no obvious  $\sigma_y$  according to ISO 527 can be detected, but in Fig. 4.3 it can be seen that  $\sigma_y$  is significantly lower, around 17.5 MPa at higher  $T$  compared to  $\sigma_y = 35.4 \pm 0.9 \text{ MPa}$  at  $T = 23 \text{ °C}$ . The results of PA12 are in accordance with results of the material data sheet -  $E = 1300 \text{ MPa}$ ,  $\epsilon_b >200 \%$  and  $\sigma_y = 39 \text{ MPa}$  at  $T = 23 \text{ °C}$ .

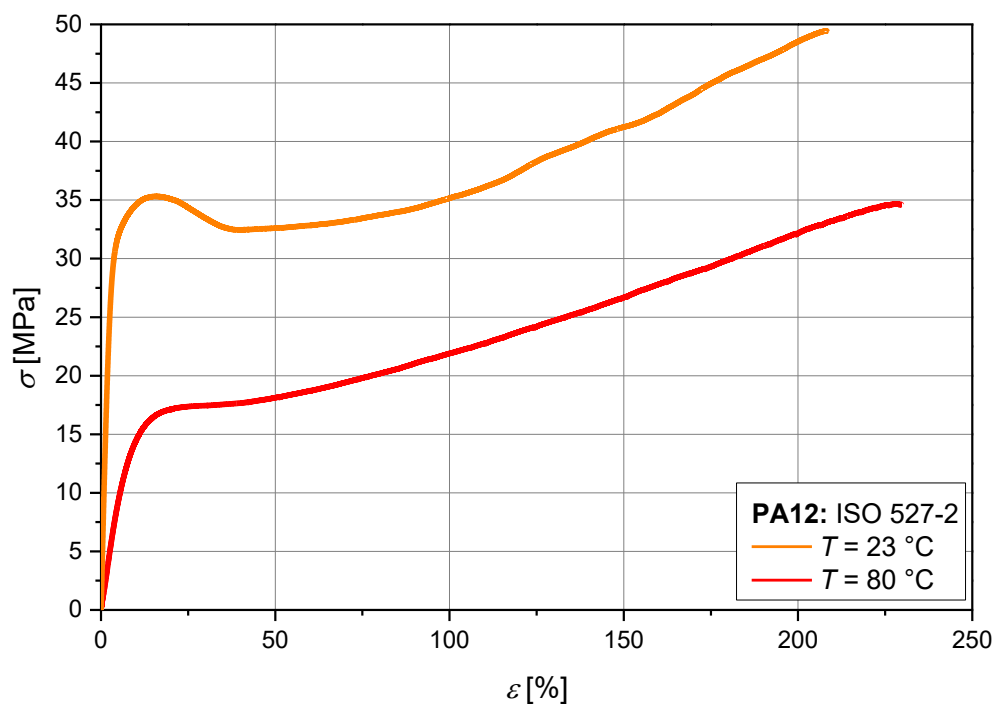


**Fig. 4.3:** Graphs of the ISO 527 tensile test of PA12 at  $T = 23^\circ\text{C}$  (orange) and  $80^\circ\text{C}$  (red).

Results of the tensile test of PE1 are representative for all three PE used in this thesis (Fig. 4.4). In the literature  $\sigma_y = 20 - 30$  MPa (Table 2.1), for the three PE's the values of  $\sigma_y$  are all within the range - PE1:  $28.9 \pm 0.5$  MPa, PE2:  $24.6 \pm 0.1$  MPa and PE3:  $27.6 \pm 0.2$  MPa. The stiffness, expressed by  $E$  is for PE1:  $912 \pm 19$  MPa, PE2:  $821 \pm 15$  MPa and PE3:  $942 \pm 46$  MPa; these values are in the lower range but agree with the reference value  $E = 800 - 1300$  MPa in Table 2.1. The results of  $\epsilon_b$  deviate considerably from the literature. The three PE types do not reach  $\epsilon_b$  of 500 %, given in literature. Specimens of PE1 break in average at a strain of  $12 \pm 1.4$  %, PE2:  $24 \pm 1.8$  % and PE3:  $17 \pm 0.7$  % (see Fig. 4.4). The dependency of  $T$  also can be recognized for PE, in Fig. 4.4 for PE1 representative for all PE types used,  $\sigma_y$  decreases from  $28.9$  MPa  $\pm 0.5$  to  $14.6$  MPa  $\pm 0.9$  as well as  $E$  ( $912$  MPa  $\pm 19$  to  $189$  MPa  $\pm 17$ ) and  $\epsilon_b$  increases from  $12$  %  $\pm 1.4$  to  $33 \pm 6$  %. These indicate that the parameters were not chosen perfectly for processing the material. For the evaluation of the SRCR-test,  $\epsilon_b$  is not taken into account in any way, so the low  $\epsilon_b$  of the specimens can be neglected. Only  $\sigma_y$  is important and this is in accordance with literature.

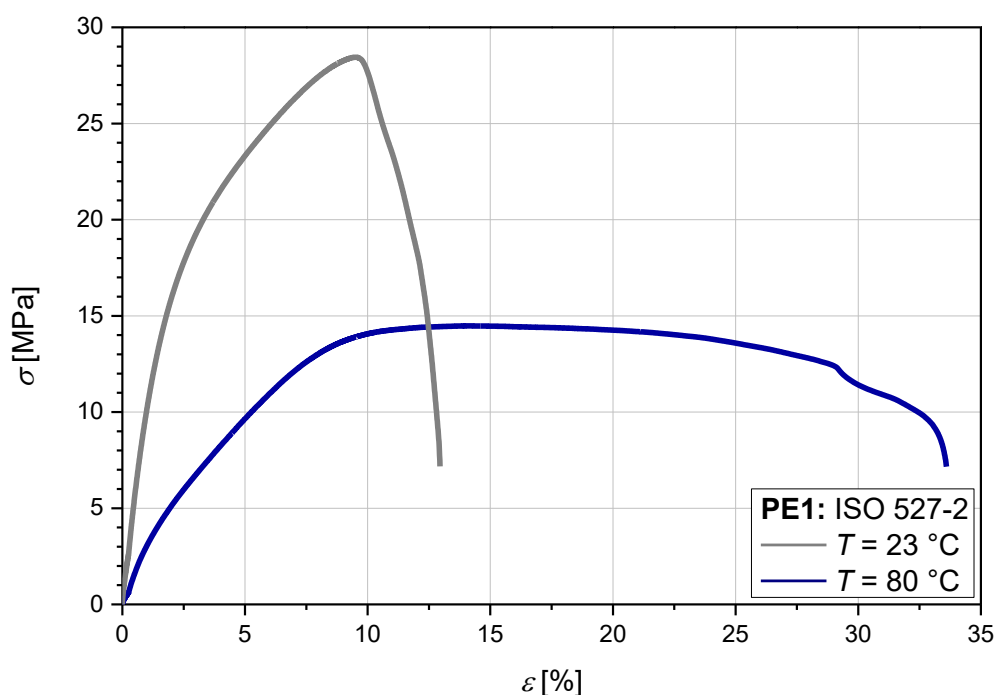


**Fig. 4.4:** Graphs of the ISO 527 tensile test of PE1, representative for all PE types used, at  $T = 23\text{ }^\circ\text{C}$  (grey) and  $80\text{ }^\circ\text{C}$  (blue).

## 4.2 Long term creep rupture behaviour

In this section the results of the individual measurements of the mSRCR method are presented. The reproducibility of the measurements and the result will be examined. Also the conditions for a valid extrapolation are investigated. Subsequently, possible improvements are discussed.

The following graphs displays the determination of  $\sigma_{y, \text{mSRCR}}$  in the  $\sigma$ - $\epsilon$  curve at different  $\dot{\sigma}$  of a test series, i.e. constant  $\sigma_{\text{ref}}$ , is shown for PA12 in Fig. 4.5 and for PE1 in Fig. 4.6, as a representative for all PE types used. The measurements of PA12 at  $\sigma_{\text{ref}} = 24\text{ MPa}$ ,  $T = 23\text{ }^\circ\text{C}$  and  $\sigma_{\text{ref}} = 13\text{ MPa}$ ,  $T = 80\text{ }^\circ\text{C}$  at different  $\dot{\sigma}$  (1, 0.1, 0.01, 0.005 and 0.001 MPa/s) were selected for Fig. 4.5. The measurement was performed until total failure of the specimen, to determine the overall deformation behaviour. The small diagram on the bottom right displays the entire curve. This diagram has been magnified for better identifying  $\sigma_{y, \text{mSRCR}}$  of each individual measurement. In Fig. 4.5 the influence of  $\dot{\sigma}$  on  $\sigma_{y, \text{mSRCR}}$  can be seen – by increasing  $\dot{\sigma}$  also  $\sigma_{y, \text{mSRCR}}$  increases. This correlation is well-known (Eyring, 1936), particularly for uniaxial tensile loadings where plasticity occurs as a function of time in thermoplastic materials. Results demonstrate the validity of the yield stress

dependency on the loading rate, despite preloading the material up to an initial  $\sigma_{\text{ref}}$ . Therefore, it is possible to extrapolate the failure behaviour of PA12.

As  $\sigma_{y, \text{mSRCR}}$  is also influenced by  $T$ , measurements for PA12 at  $\dot{\sigma} < 0.005$  MPa/s or at elevated temperature of  $T = 80$  °C are not evaluable with this method, since no obvious  $\sigma_{y, \text{mSRCR}}$  can be determined, which is the prerequisite for the evaluation of the mSRCR-test. For PA12 the glass transition temperature  $T_g$  according to the data sheet is at  $T_g = 36$  °C and the material is normally used below  $T_g$ . The measurements at  $T = 80$  °C are above  $T_g$  and the deformation behaviour is different. Yielding occurs during the measurements, but no clear  $\sigma_y$  is visible. This, on the other hand, also corresponds to ISO 527 results at elevated temperatures. For the analysis of this measurements, the evaluation method of the mSRCR-test must be further adapted based on different failure criteria than  $\sigma_y$ .

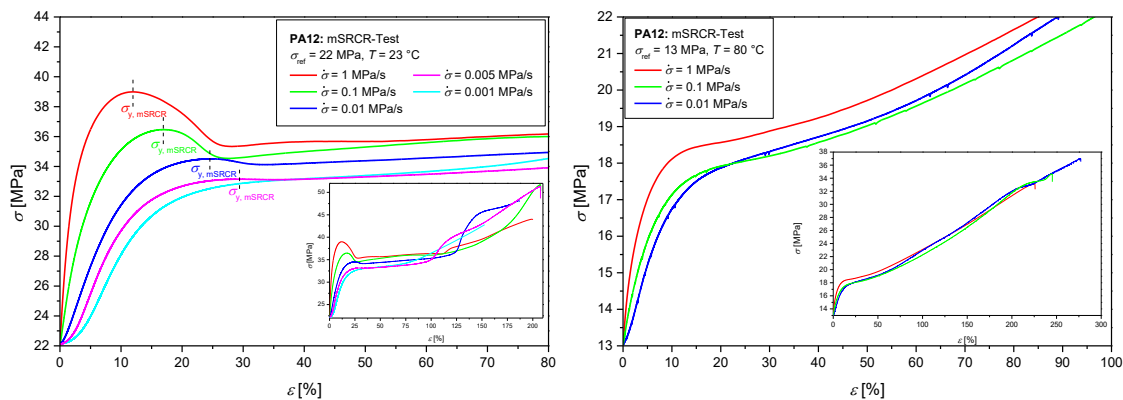


**Fig. 4.5:** Measurements and determination of  $\sigma_{y, \text{mSRCR}}$  for PA12 at different  $\dot{\sigma}$  and  $\sigma_{\text{ref}} = 24$  MPa for  $T = 23$  °C (left) and  $\sigma_{\text{ref}} = 13$  MPa for  $T = 80$  °C (right) in a magnified view. On the bottom right, the entire curve.

The measurements of PE1 at different  $\dot{\sigma}$  at  $\sigma_{\text{ref}} = 12.5$  MPa,  $T = 23$  °C and  $\sigma_{\text{ref}} = 5.5$  MPa,  $T = 80$  °C are displayed in Fig. 4.6. In the literature,  $T_g$  for HDPE is  $-120$  °C  $< T_g < -80$  °C (Domininghaus et al., 2012), both test temperatures are far above  $T_g$ , the deformation behaviour is similar. The strains are significantly small compared to a typical PE ( $> 500$  %), displaying similar results as shown in tensile tests (chapter 4.1.3).

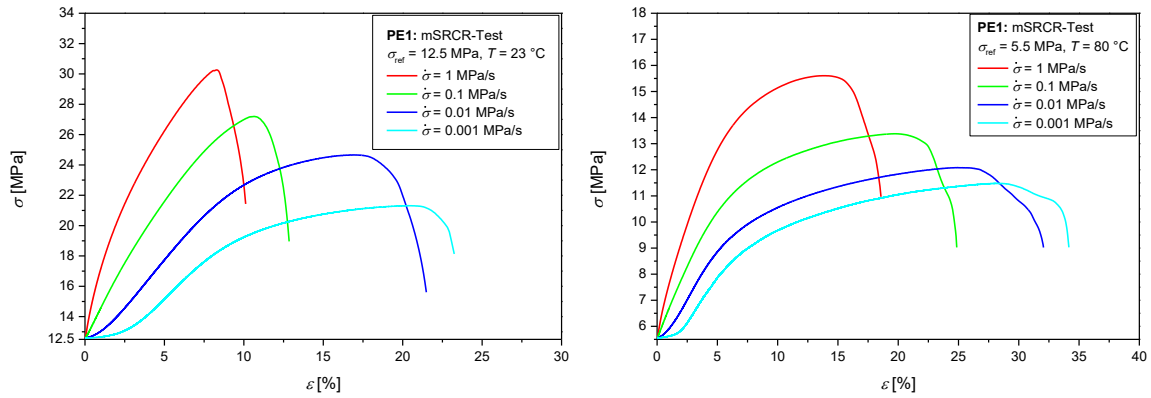


**Fig. 4.6:** Measurements of  $\sigma_{y, \text{mSRCR}}$  for PE1 at different  $\dot{\sigma}$  and  $\sigma_{\text{ref}} = 12.5 \text{ MPa}$  for  $T = 23 \text{ }^\circ\text{C}$  (left) and  $\sigma_{\text{ref}} = 5.5 \text{ MPa}$  for  $T = 80 \text{ }^\circ\text{C}$  (right).

The mean values and standard deviation of  $\sigma_{y, \text{mSRCR}}$  and  $t_{y, \text{mSRCR}}$  for each measurement, at different  $\sigma_{\text{ref}}$  and  $\dot{\sigma}$  for all pipe grades are summarized in the following four figures Fig. 4.7 - Fig. 4.10. Due to the small differences between the data at various  $\sigma_{\text{ref}}$ , different symbols for various  $\sigma_{\text{ref}}$  in Fig. 4.8 - Fig. 4.10 have been omitted for a better representation. Since the number of specimens of PE2 and PE3 was limited, the tests at  $T = 80 \text{ }^\circ\text{C}$  was only performed at three levels of stress rates ( $\dot{\sigma} = 1 \text{ MPa/s}$ ,  $0.1 \text{ MPa/s}$  and  $0.01 \text{ MPa/s}$ ). The double-logarithmic diagrams represent the evaluated  $\sigma_{y, \text{mSRCR}}$  and  $t_{y, \text{mSRCR}}$  as a function of  $\sigma_{\text{ref}}$  and  $\dot{\sigma}$ . A linear relationship between  $\sigma_{y, \text{mSRCR}}$  and  $t_{y, \text{mSRCR}}$  can be determined. It is evident, that due to the plastic deformation mechanism of the material and the strong influence of  $\dot{\sigma}$  and  $T$  on  $\sigma_{y, \text{mSRCR}}$  with increasing  $\sigma_{\text{ref}}$  and constant stress rate ( $\dot{\sigma}$ )  $t_{y, \text{mSRCR}}$  decreases, while an increase gets observable with decreasing  $\dot{\sigma}$ . For PA12 in Fig. 4.7, several markers are used to illustrate the influence of  $\sigma_{\text{ref}}$ . At a low  $\sigma_{\text{ref}}$ ,  $t_{y, \text{mSRCR}}$  is higher compared to lower  $\sigma_{\text{ref}}$  at a specific  $\dot{\sigma}$ . The influence of  $\sigma_{\text{ref}}$  on the yield stress ( $\sigma_{y, \text{mSRCR}}$ ) at a certain  $\dot{\sigma}$  is not significant,  $\sigma_{y, \text{mSRCR}}$  are all of the same order ( $\pm 1 \text{ MPa}$ ). In summary, it can be noted that the specific reference stress level  $\sigma_{\text{ref}}$  has a non-significant influence on the yield stress ( $\sigma_{y, \text{mSRCR}}$ ) but a high influence on the time until the yield stress is reached ( $t_{y, \text{mSRCR}}$ ). The scattering of the individual measurements is very small ( $<4 \%$ ), concluding a high reproducibility of the measurements. For PE1 in Fig. 4.8, the distance between different  $\sigma_{\text{ref}}$  were chosen smaller, compared to PA12 (Table 3.1). The influence of  $\sigma_{\text{ref}}$  on  $t_{y, \text{mSRCR}}$  is no longer visible at both temperatures. At  $T = 80 \text{ }^\circ\text{C}$  the dependence of  $\sigma_{y, \text{mSRCR}}$  on  $\sigma_{\text{ref}}$  is

higher, this may be due to machine inaccuracies, as  $\sigma_{\text{ref}}$  distances were chosen too small. The two further PE materials, PE2 and PE3, are summarized in Fig. 4.9 and Fig. 4.10 and show similar characteristics in their results as material PE1.

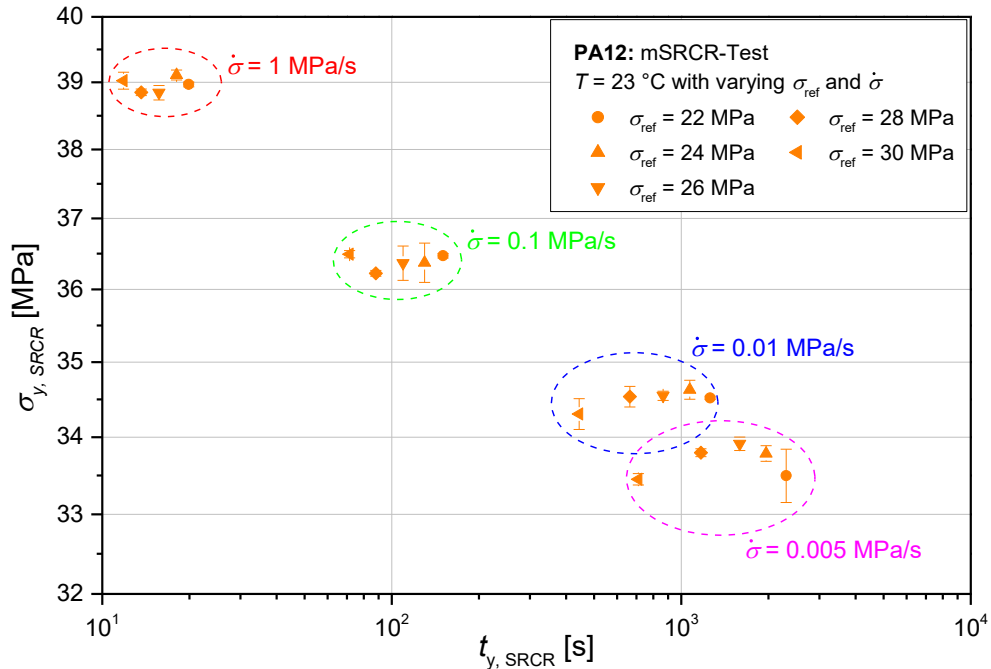


**Fig. 4.7:** Results of the measurements of PA12 at varying  $\sigma_{\text{ref}}$  and  $\dot{\sigma}$  at  $T = 23 \text{ }^\circ\text{C}$ .

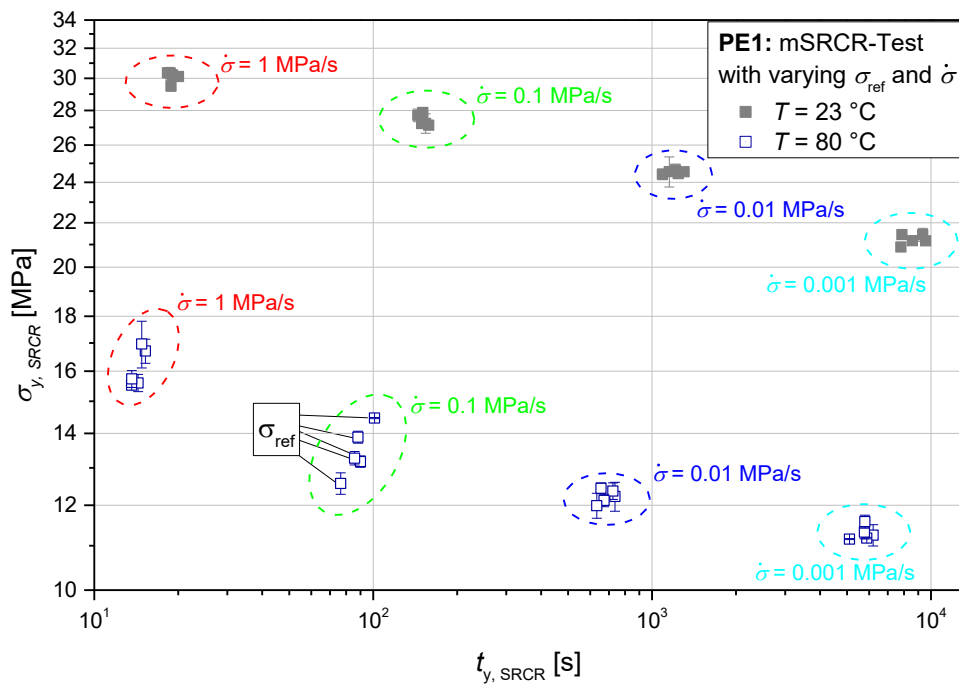


**Fig. 4.8:** Results of the measurements of PE1 at varying  $\sigma_{\text{ref}}$  and  $\dot{\sigma}$  at  $T = 23 \text{ }^\circ\text{C}$  (grey, closed markers) and  $80 \text{ }^\circ\text{C}$  (blue, open markers).



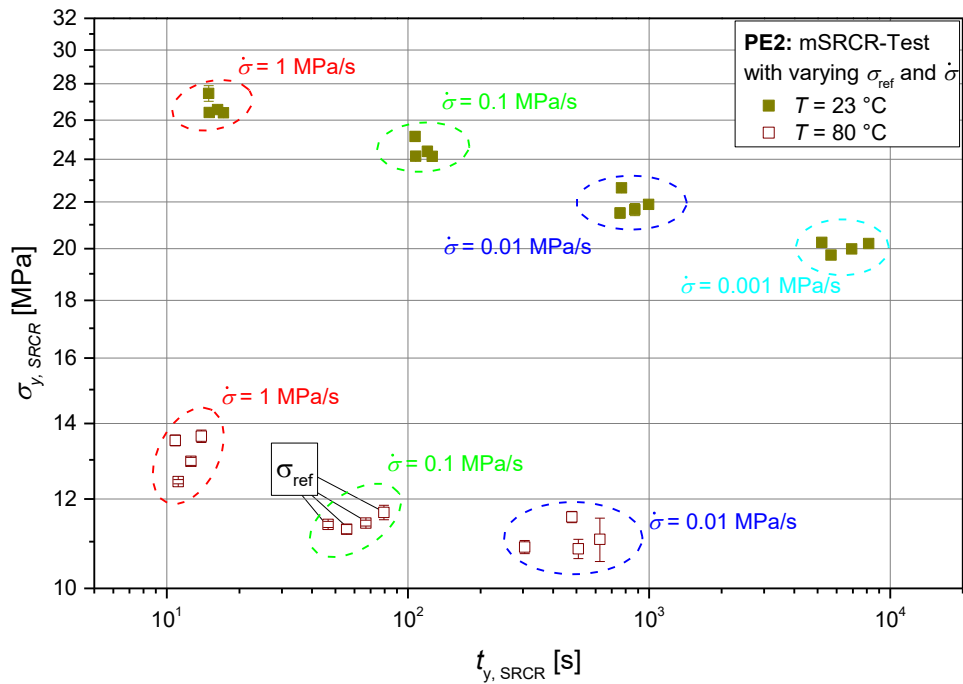


**Fig. 4.9:** Results of the measurements of PE2 at varying  $\sigma_{\text{ref}}$  and  $\dot{\sigma}$  at  $T = 23\text{ °C}$  (olive, closed markers) and  $80\text{ °C}$  (brown, open markers).

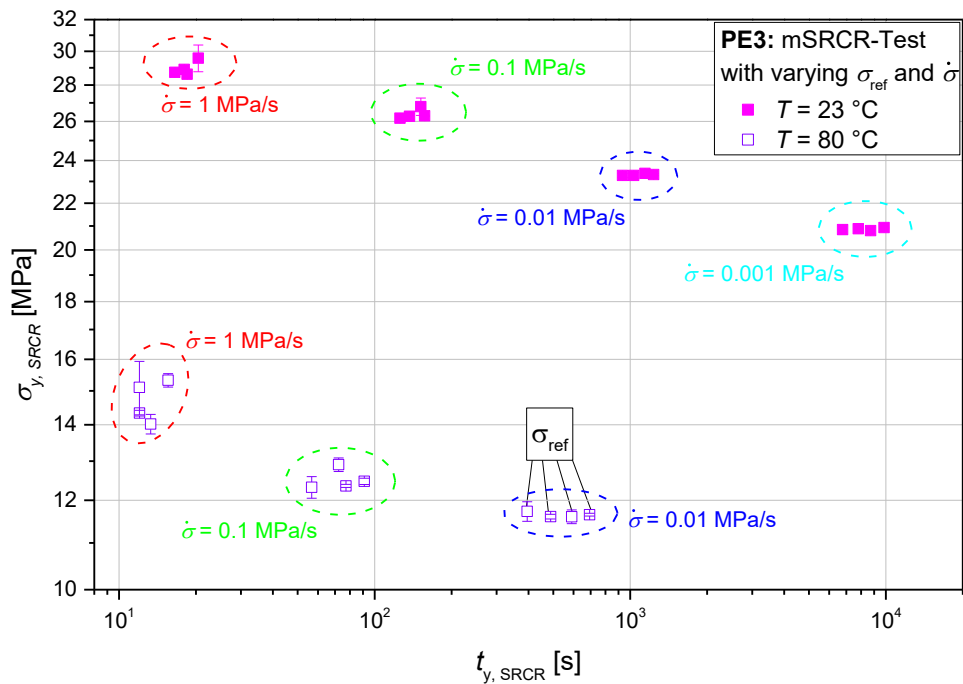


**Fig. 4.10:** Results of the measurements of PE3 at varying  $\sigma_{\text{ref}}$  and  $\dot{\sigma}$  at  $T = 23\text{ °C}$  (pink, closed markers) and  $80\text{ °C}$  (violet, open markers).

To extend the applicability of the classical SRCR-test used for reinforced thermoplastics, which display obvious brittle failure, towards non-reinforced, tough materials, which display a plasticity controlled failure behaviour, it is necessary to investigate whether there is a correlation between  $\sigma_{y, \text{mSRCR}}$  and  $\dot{\sigma}$  (Eyring, 1936; Bauwens-Crowet et al., 1974). For this purpose,  $\sigma_{y, \text{mSRCR}}$  of the different materials were plotted as a function of  $\dot{\sigma}$  at each temperature ( $T = 23 \text{ }^\circ\text{C}$  and  $80 \text{ }^\circ\text{C}$ ). In the following diagrams Fig. 4.11 - Fig. 4.14, the dependence of  $\sigma_{y, \text{mSRCR}}$  on  $\dot{\sigma}$  for PA12, PE1, PE2 and PE3 is illustrated. It should be noted, that only the x-axis ( $\dot{\sigma}$ ) is displayed logarithmically.

For PA12 the measurements are shown for one temperature  $T = 23 \text{ }^\circ\text{C}$  only. As described above,  $\sigma_{y, \text{mSRCR}}$  is strongly dependent on  $\dot{\sigma}$  ( $\sigma_{y, \text{mSRCR}}$  increases with increasing  $\dot{\sigma}$ ). The dependency, which must be given according to literature (Bauwens-Crowet et al., 1974) to extrapolate the deformation mechanism, is clearly visible in the following diagrams. At a temperature of  $T = 23 \text{ }^\circ\text{C}$  a linear correlation is present for all materials. This linear correlation confirms that the failure behaviour can be extrapolated. Despite  $\sigma_{\text{ref}}$  this correlation is still given. At higher temperature  $T = 80 \text{ }^\circ\text{C}$ , no linear correlation is apparent for the different tested PE types. The curve shows two different slopes, the slope at higher  $\dot{\sigma}$  is parallel to the slope at  $T = 23 \text{ }^\circ\text{C}$ . The phenomenon of the different slopes at higher  $T$  is well known in literature and indicates two different deformation processes, each of contributes to  $\sigma_{y, \text{mSRCR}}$  (Bowden and Young, 1974; Roetling, 1966; Hiss et al., 1999). The slope at higher  $T$  and lower  $\dot{\sigma}$  is flatter, due to the negligible contribution of the interlamellar deformation processes (process II, chapter 2.2.1), only intralamellar deformation processes contribute to  $\sigma_{y, \text{mSRCR}}$ . For the materials PE2 and PE3 only three different  $\dot{\sigma}$  have been measured, but a change in the slope can be clearly observed. By additional measurements at lower  $\dot{\sigma}$ , the statement which is currently based on only three measuring points can be reviewed. In this illustration, the low dependence of  $\sigma_{y, \text{mSRCR}}$  on  $\sigma_{\text{ref}}$  can also be recognized.

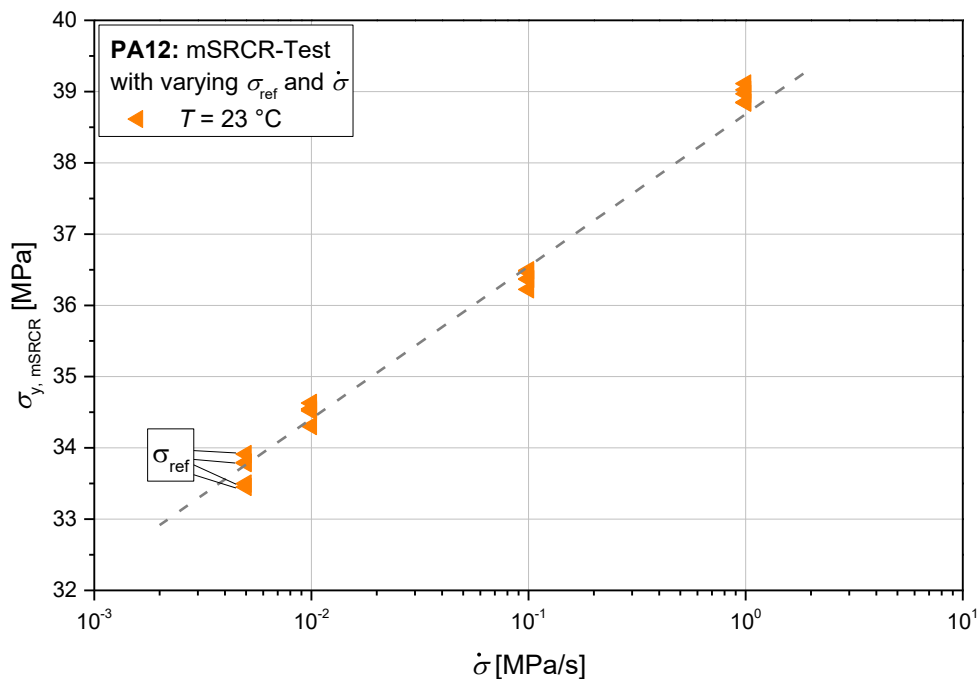


**Fig. 4.11:** The dependence of  $\sigma_{y, \text{mSRCR}}$  on  $\dot{\sigma}$  at  $T = 23 \text{ }^\circ\text{C}$  and variable  $\sigma_{\text{ref}}$  for PA12.

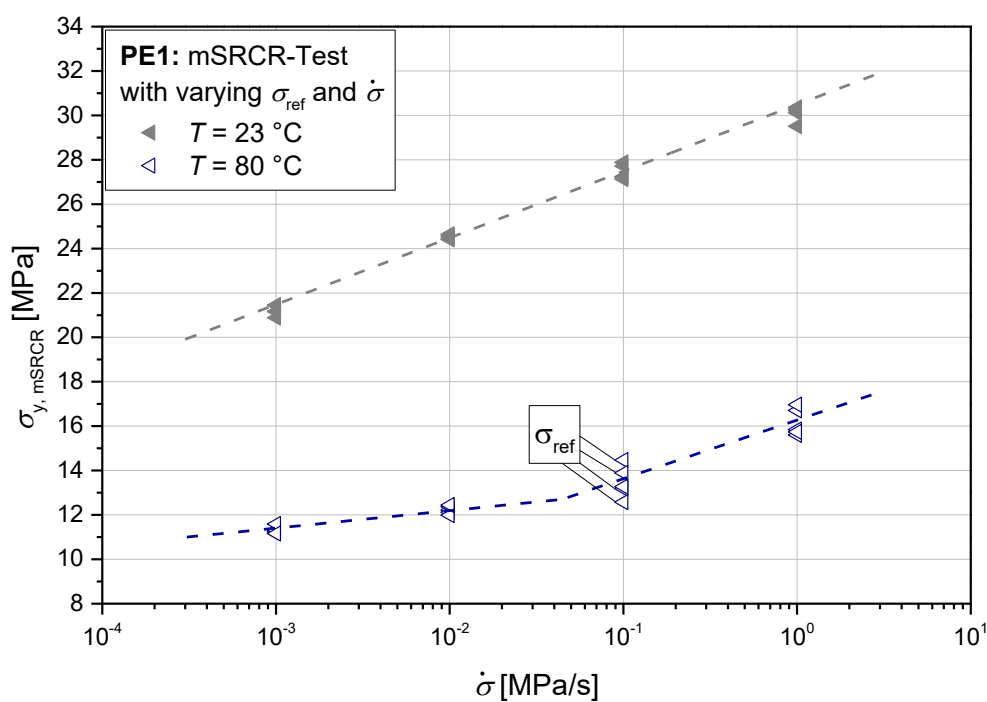


**Fig. 4.12:** The dependence of  $\sigma_{y, \text{mSRCR}}$  on  $\dot{\sigma}$  and variable  $\sigma_{\text{ref}}$  at  $T = 23 \text{ }^\circ\text{C}$  (grey, closed markers) and  $T = 80 \text{ }^\circ\text{C}$  (blue, open markers) and variable  $\sigma_{\text{ref}}$  for PE1.

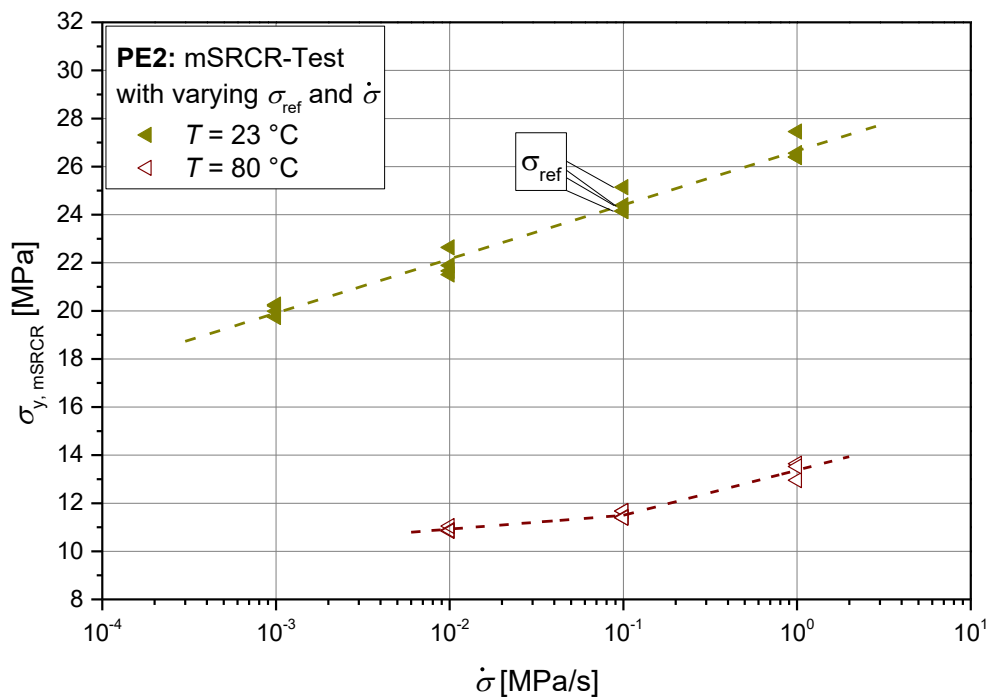


**Fig. 4.13:** The dependence of  $\sigma_{y, mSRCR}$  on  $\dot{\sigma}$  and variable  $\sigma_{ref}$  at  $T = 23 \text{ }^{\circ}\text{C}$  (olive, closed markers) and  $T = 80 \text{ }^{\circ}\text{C}$  (brown, open markers) and variable  $\sigma_{ref}$  for PE2.

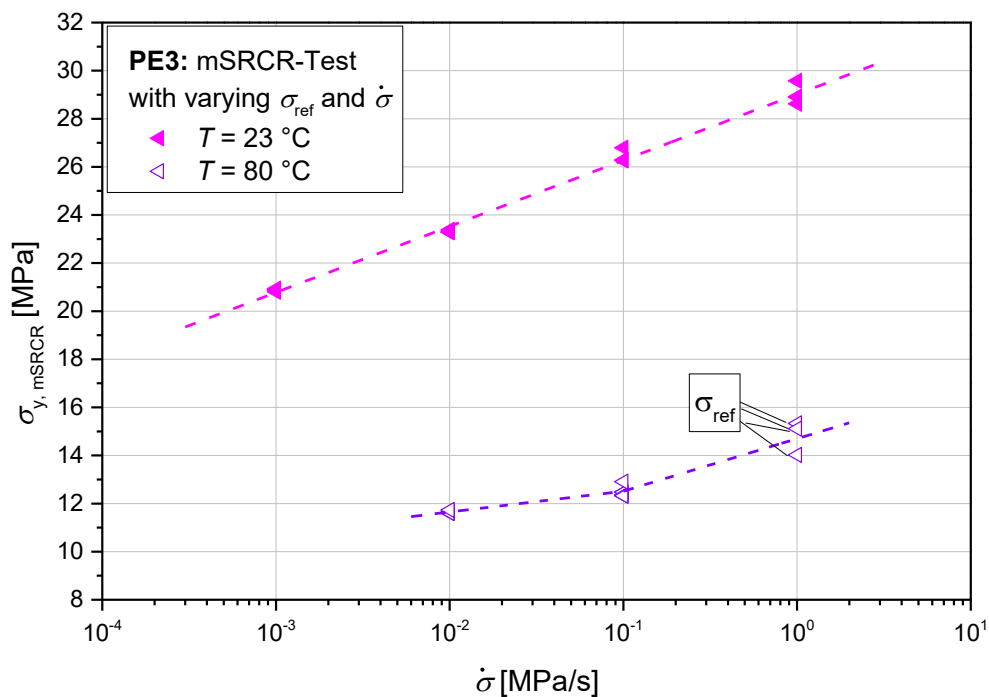


**Fig. 4.14:** The dependence of  $\sigma_{y, mSRCR}$  on  $\dot{\sigma}$  and variable  $\sigma_{ref}$  at  $T = 23 \text{ }^{\circ}\text{C}$  (pink, closed markers) and  $T = 80 \text{ }^{\circ}\text{C}$  (violet, open markers) and variable  $\sigma_{ref}$  for PE3.

A correlation between  $\sigma_{y, mSRCR}$  and  $\sigma$  is found in the semi-logarithmic diagrams, thus the failure behaviour of the individual measurements can be extrapolated in order to create the extrapolated Stage I failure curves for the different materials. The long-term strength behaviour of PA12, PE1, PE2 and PE3 is shown in Fig. 4.15 - Fig. 4.18, respectively. In order to determine the Stage I failure curve, the double-logarithmic diagram shows the extrapolated  $t_f$  at the different static reference loads  $\sigma_{ref}$ . For comparison with ISO 9080 and to determine the mSRCR based MRS value, the strength after 50 years  $\sigma_{50a, mSRCR}$  was determined for each material and temperature  $T$  ( $T = 23\text{ °C}$  and  $80\text{ °C}$ ). For PA12 the data points correspond to the expectations -  $t_f$  increases with decreasing  $\sigma_{ref}$  and a linear correlation can be drawn resulting in a predicted strength of  $\sigma_{50a, mSRCR} = 22.5\text{ MPa}$  at  $T = 23\text{ °C}$ .

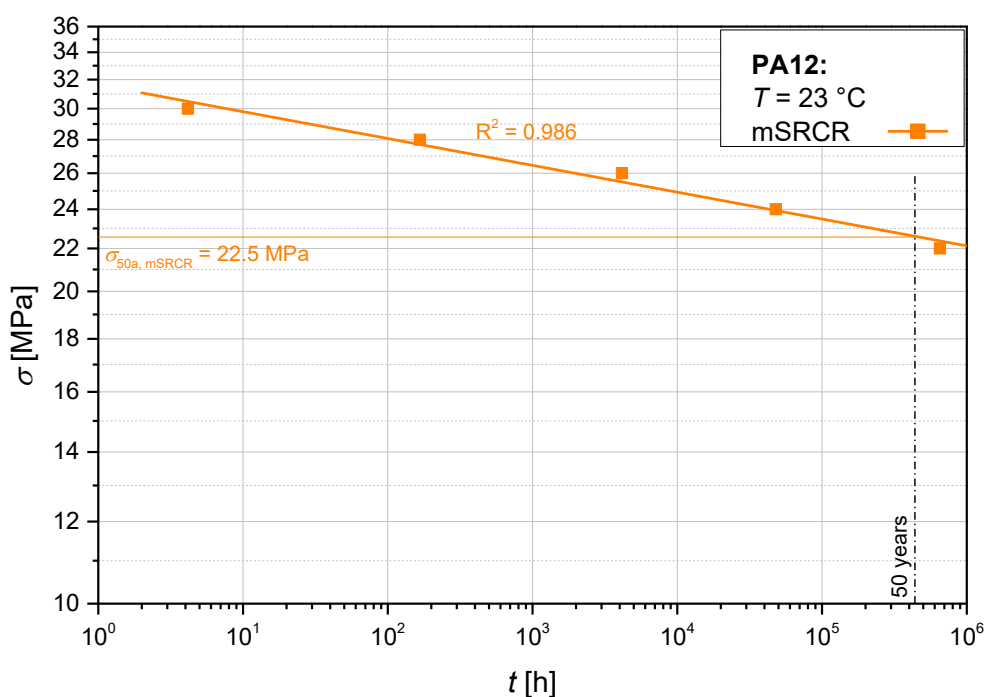


**Fig. 4.15:** Result of the mSRCR-test, i.e. the long-term strength behaviour of PA12 at  $T = 23\text{ °C}$ .

Slopes of the linear regressions for PE1, PE2 and PE3 at different  $T$  are approximately parallel, which indicates the same failure mechanism (yielding) at both  $T$ . For every PE (Fig. 4.16 - Fig. 4.18), the coefficient of determination  $R^2$  of the linear correlation is lower at higher  $T$ . With increasing  $T$ ,  $R^2$  also decreases, and the extrapolations are not as accurate and the deviation rises. There are some predicted times that do not follow the schema, that at higher applied reference stresses  $\sigma_{ref}$

the time until failure  $t_f$  decreases. This especially occurs for PE1 at both temperature  $T = 23\text{ }^\circ\text{C}$ , (at  $\sigma_{\text{ref}} = 11.5\text{ MPa}$  is shorter  $t_f$  than at  $\sigma_{\text{ref}} = 12\text{ MPa}$ ) and  $80\text{ }^\circ\text{C}$  (for  $\sigma_{\text{ref}} = 5.25$  and  $\sigma_{\text{ref}} = 6\text{ MPa}$ , whereas for PE2 and PE3 this occurs only at higher temperature ( $T = 80\text{ }^\circ\text{C}$ ). As described in chapter 2.2.2,  $t_f$  should be higher at lower applied stresses. These two extrapolated data points must be checked with further measurements. In addition, for PE1 the gap between the  $\sigma_{\text{ref}}$  has been chosen smaller compared to the measurements at  $T = 23\text{ }^\circ\text{C}$ . Unfortunately, the fluctuations of the machine when applying  $\sigma_{\text{ref}}$  might be in a range that the values overlap at these small gaps. For PE1 the extrapolation resulted in  $\sigma_{50a, \text{mSRCR}} = 11.40\text{ MPa}$  at  $T = 23\text{ }^\circ\text{C}$  and  $\sigma_{50a, \text{mSRCR}} = 5.47\text{ MPa}$  at  $T = 80\text{ }^\circ\text{C}$ .

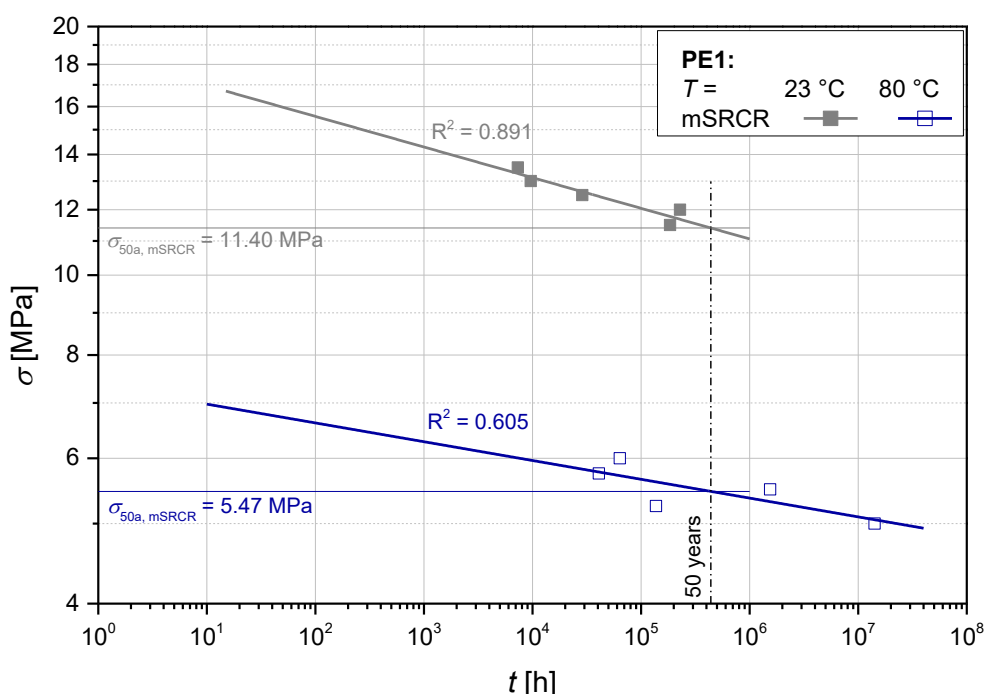


**Fig. 4.16:** Result of the mSRCR-test, i.e. the long-term strength behaviour of PE1 at  $T = 23\text{ }^\circ\text{C}$  (grey, closed markers) and  $T = 80\text{ }^\circ\text{C}$  (blue, open markers).

In Fig. 4.17 the long-term strength behaviour of PE2 is illustrated with  $\sigma_{50a, \text{mSRCR}} = 11.80\text{ MPa}$  at  $T = 23\text{ }^\circ\text{C}$  and  $\sigma_{50a, \text{mSRCR}} = 5.98\text{ MPa}$  at  $T = 80\text{ }^\circ\text{C}$ . The extrapolation of the different measurements at  $\sigma_{\text{ref}} = 7\text{ MPa}$  and  $T = 80\text{ }^\circ\text{C}$  has resulted in a higher  $t_f$ , the other points are following the expectations ( $t_f$  increases at lower  $\sigma_{\text{ref}}$ ). The deviation of this point compared to the other data points is very high, so  $R^2$  is also reduced and  $\sigma_{50a, \text{mSRCR}}$  is increased. In an additional calculation this point was not considered because of the high deviation. The extrapolation was

carried out only with the points at  $\sigma_{\text{ref}} = 8 \text{ MPa}$ ,  $6 \text{ MPa}$  and  $5 \text{ MPa}$ . By neglecting the point at  $\sigma_{\text{ref}} = 7 \text{ MPa}$ , a  $\sigma_{50a, \text{mSRCR}}$  of  $5.11 \text{ MPa}$  is obtained with an  $R^2 = 0.968$  of the linear correlation. In the following evaluation and discussion, the point at  $\sigma_{\text{ref}} = 7 \text{ MPa}$  is considered, but it should be critically examined and checked by additional measurements. The extrapolated point shows the current deficiencies of the modified method, which should be considered in further development.

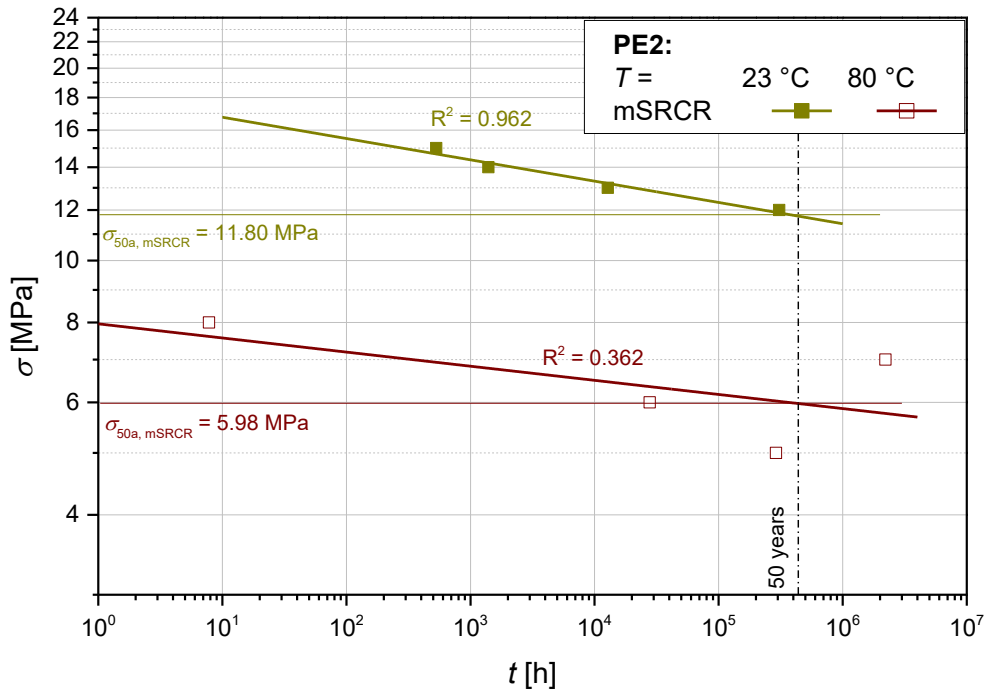


**Fig. 4.17:** Result of the mSRCR-test, i.e. the long-term strength behaviour of PE2 at  $T = 23 \text{ °C}$  (olive, closed markers) and  $T = 80 \text{ °C}$  (brown, open markers).

The long-term strength for PE3 (Fig. 4.18) was extrapolated to a strength after 50 years of  $\sigma_{50a, \text{mSRCR}} = 10.80 \text{ MPa}$  at  $T = 23 \text{ °C}$  and to  $\sigma_{50a, \text{mSRCR}} = 5.02 \text{ MPa}$  at  $T = 80 \text{ °C}$ . As already mentioned, the  $R^2$  is lower at higher  $T$ . In this linear regression at  $T = 80 \text{ °C}$ , all points were taken into account, since it is difficult to determine whether the point at  $\sigma_{\text{ref}} = 6 \text{ MPa}$  or  $5 \text{ MPa}$  is an outlier. If  $\sigma_{\text{ref}} = 6 \text{ MPa}$  is the outlier, the regression would shift to a lower  $\sigma_{50a, \text{mSRCR}}$ . If, on the other hand, if  $\sigma_{\text{ref}} = 5 \text{ MPa}$  is an outlier, this would lead to a higher long-term strength.

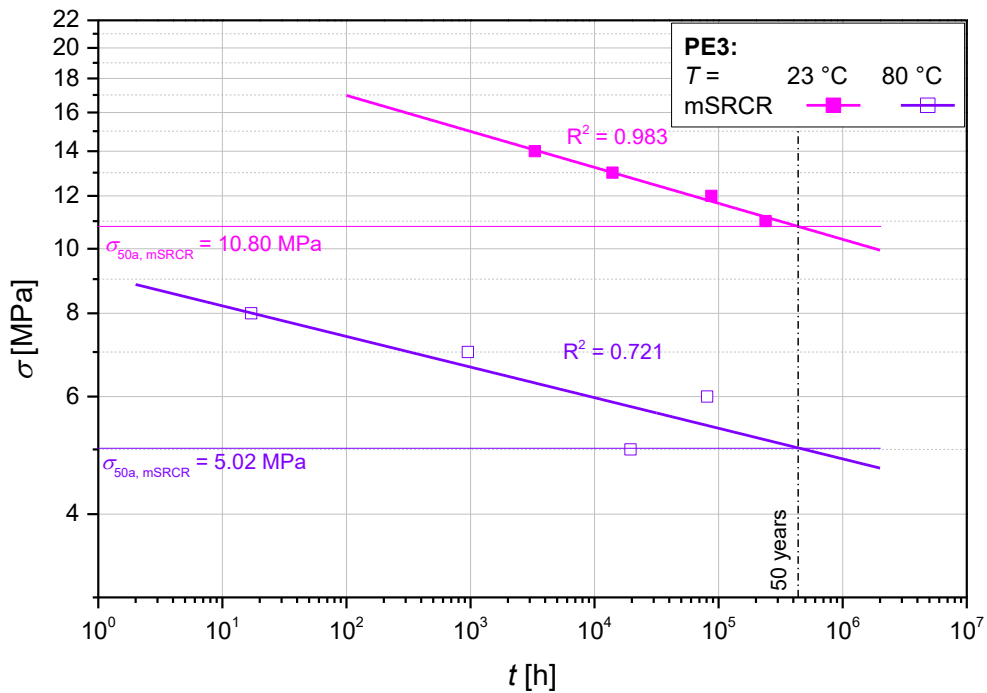


**Fig. 4.18:** Result of the mSRCR-test, i.e. the long-term strength behaviour of PE3 at  $T = 23\text{ }^\circ\text{C}$  (pink, closed markers) and  $T = 80\text{ }^\circ\text{C}$  (violet, open markers).

The extrapolated data points, on which currently no exact statement can be made whether the point is an outlier or not, must be checked with further measurements. The load during the test causes irreversible micro-damage, which can occur before  $\sigma_y$  is reached. These micro-damages, leading to plastic deformation take place at the beginning of the non-linear viscoelastic deformation area and cannot be measured by conventional tensile tests (Grellmann and Seidler, 2011).

Deviations can be attributed to different influences on specimens and measurements. Due to the fact that a certain statistical scattering of the measured parameters  $\sigma_{y, \text{mSRCR}}$  and  $t_{y, \text{mSRCR}}$  generally occurs, deviation may occur. However, the deviations of the measurements are very small as can be seen in Fig. 4.7 - Fig. 4.10.

During manufacturing micro-damages can already be introduced into the material, which can lead to lower strength behaviour (Grellmann and Seidler, 2011). Moreover, the specimen conditioning or the clamping can have an effect to the results. At higher  $T$  the effect of the clamping has a high influence on the



measurements, as slipping effects occur due to the higher affinity of the material to yielding, which leads to lower clamping forces.

In summary, the mSRCR-test method is a basis to determine a Stage I failure curve and to predict the long-term strength of thermoplastic materials but there are still a lot of questions. To improve the accuracy of data points, which currently do not reach the expectation that at higher applied stresses ( $\sigma_{\text{ref}}$ ) the time until failure ( $t_f$ ) is shorter than at lower stresses, the number of measurements per load condition as well as the number of different reference stress levels  $\sigma_{\text{ref}}$  and stress rates  $\dot{\sigma}$  should be enhanced. As test results displayed a non-typical behaviour in terms of  $\epsilon_b$ , the influence of specimen manufacturing must be critically examined. But in this case for the extrapolation of the method,  $\epsilon_b$  is not considered, so the low  $\epsilon_b$  of the specimens can be neglected. Additional creep tests can confirm the predicted failure curves of the mSRCR-test. No creep tests were carried out in the present thesis.

### 4.3 Comparison to internal pipe pressure test

To obtain feasible stress values for applying the mSRCR-test method to PA12, PE1, PE2 and PE3 pipes, results of the internal pipe pressure test ISO 9080 were used as reference. However, to compare this multiaxial test with an uniaxial test, the results were converted to an equivalent stress. Results and deviations are summarized in Table 4.2. Two hypotheses for determination of the equivalent stress were used. The first one is according to von Mises ( $\sigma_{\text{VM}} = \frac{\sqrt{3}}{2} \sigma_h$ ) and the second according to Tresca ( $\sigma_T = \sigma_h$ ) (chapter 2.4). In each case, the deviation from  $\sigma_{50a, \text{mSRCR}}$  to the equivalent stress  $\sigma_{50a, T}$  and  $\sigma_{50a, \text{VM}}$  was calculated. The deviation of  $\sigma_{50a, \text{mSRCR}}$  to  $\sigma_{50a, \text{VM}}$  is higher because the values of  $\sigma_h$  are only reduced by a factor of  $\frac{\sqrt{3}}{2}$ .

In the following figures Fig. 4.19 - Fig. 4.22 the results of the internal pipe pressure test (ISO 9080) and mSRCR-test are compared to each other. For a better understanding,  $\sigma_{\text{LTHS}}$  (equal to  $\sigma_{50a, T}$ ) and  $\sigma_{50a, \text{mSRCR}}$  are given in the following graphs at the specific temperatures. Additionally, the results with the von Mises criterion are illustrated. The slopes of the results, calculated with the equivalent

stresses  $\sigma_T$  and  $\sigma_{VM}$ , are parallel, as the stress values have only been shifted by a factor of  $\frac{\sqrt{3}}{2}$  (chapter 2.4.1).

**Table 4.2:** Results and deviation of mSRCR-test  $\sigma_{50a, mSRCR}$  and ISO 9080 ( $\sigma_{50a, T}$  and  $\sigma_{50a, VM}$ ) for PA12, PE1, PE2 and PE3.

Material	T [°C]	Long-term strength $\sigma_{50a}$ [MPa]		Deviation of $\sigma_{50a, mSRCR}$ [%]
		$\sigma_{mSRCR}$		
PA12	23	$\sigma_{mSRCR}$	22.56	-
		$\sigma_T$	20.24	11.7
		$\sigma_{VM}$	17.53	28.7
PE1	23	$\sigma_{mSRCR}$	11.40	-
		$\sigma_T$	11.14	2.4
		$\sigma_{VM}$	9.65	18.2
	80	$\sigma_{mSRCR}$	5.47	-
		$\sigma_T$	5.45	0.3
		$\sigma_{VM}$	4.72	15.8
PE2	23	$\sigma_{mSRCR}$	11.80	-
		$\sigma_T$	10.83	8.9
		$\sigma_{VM}$	9.38	25.7
	80	$\sigma_{mSRCR}$	5.11	-
		$\sigma_T$	5.42	5.7
		$\sigma_{VM}$	4.70	8.9
PE3	23	$\sigma_{mSRCR}$	10.80	-
		$\sigma_T$	10.81	0.2
		$\sigma_{VM}$	9.36	15.3
	80	$\sigma_{mSRCR}$	5.02	-
		$\sigma_T$	5.24	4.2
		$\sigma_{VM}$	4.54	10.6

For PA12 (Fig. 4.19) the results of the extrapolated long-term strength behaviour are almost identical with the internal pipe pressure test at higher applied stresses. With decreasing the applied stress the deviation between the mSRCR-test and the internal pipe pressure test increases. In Fig. 4.19 it can be seen that the slope of the mSRCR-test is different compared to the internal pipe pressure test results.

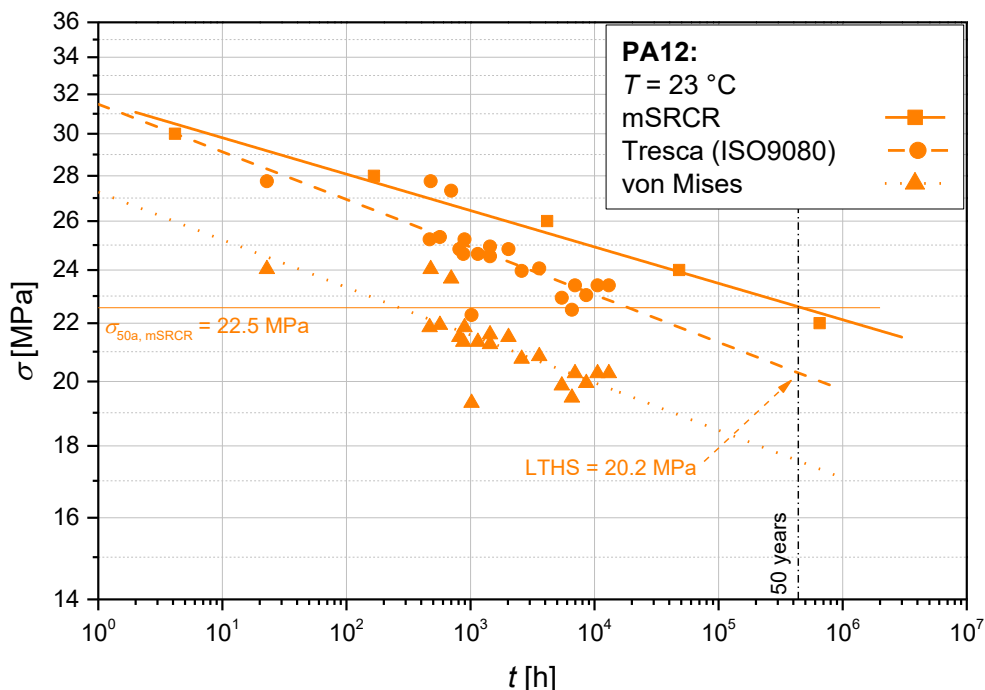


**Fig. 4.19:** Comparison of the mSRCR-test with the equivalent stresses of ISO 9080 for PA12 at  $T = 23 \text{ }^{\circ}\text{C}$ .

The results show that for the different PE types Fig. 4.20 - Fig. 4.21,  $\sigma_{50a, \text{mSRCR}}$  is almost identical with  $\sigma_{\text{LTHS}}$ . However, due to the different slopes of the failure curves the deviation increases when comparing the strength at lower  $t_f$ , i.e. for PE1 at  $t_f = 10 \text{ years}$  and  $T = 23 \text{ }^{\circ}\text{C}$ ,  $\sigma_{10a, \text{mSRCR}}$  results to 12.11 MPa and  $\sigma_{10a, T}$  is 11.54 MPa, the deviation is 5 %. This rather indicates an incidental accordance of the values. Nonetheless, it should be noted that two different test methods and stress states are compared here - for the internal pipe pressure test extruded pipes are used, while injection moulded multipurpose specimens were tested via mSRCR. The comparison and results should be considered critically. The crystallinity, geometry, stress states, internal stresses and orientations of the chains in the specimen can have a big influence on the results. For further developments the influences of the factors mentioned above are to be investigated additionally.

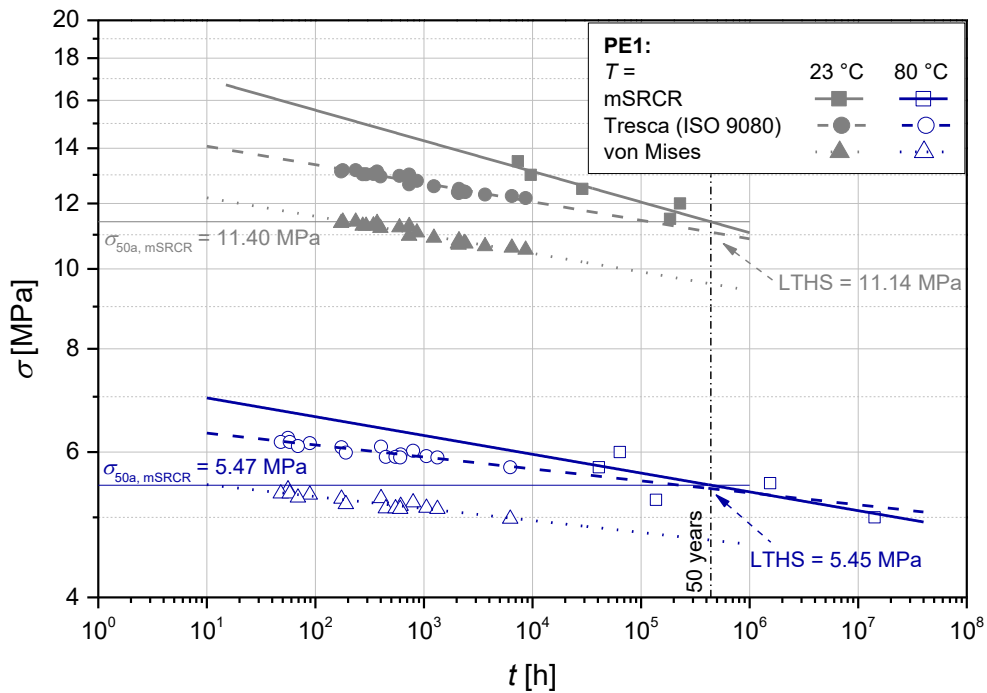


**Fig. 4.20:** Comparison of the mSRCR-test with the equivalent stresses of ISO 9080 for PE1 at  $T = 23^\circ\text{C}$  (grey, closed markers) and  $T = 80^\circ\text{C}$  (blue, open markers).

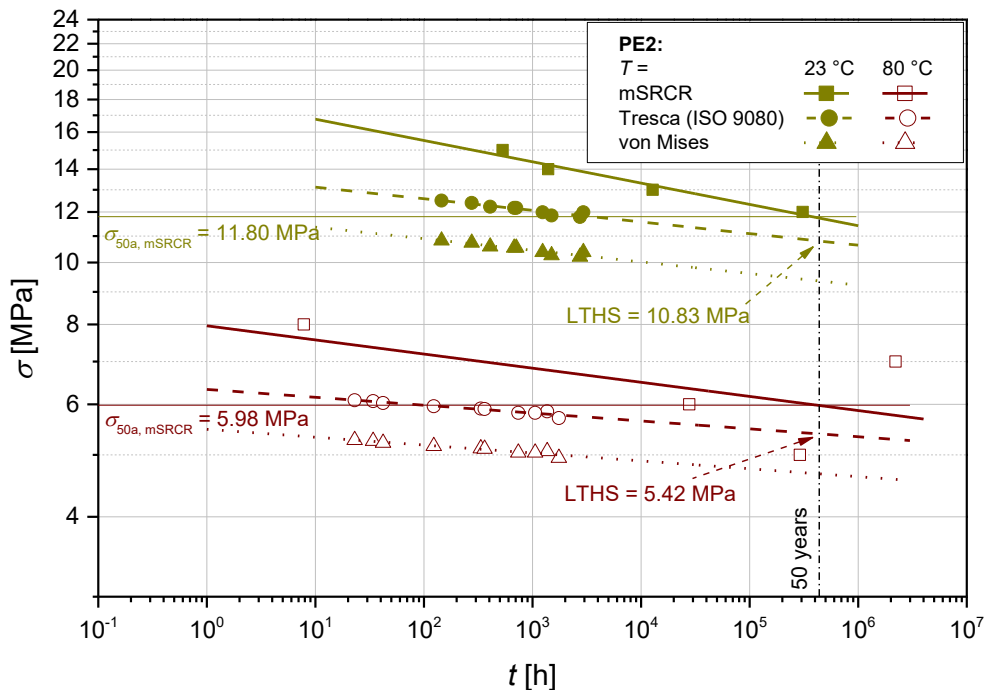


**Fig. 4.21:** Comparison of the mSRCR-test with the equivalent stresses of ISO 9080 for PE2 at  $T = 23^\circ\text{C}$  (olive, closed markers) and  $T = 80^\circ\text{C}$  (brown, open markers).

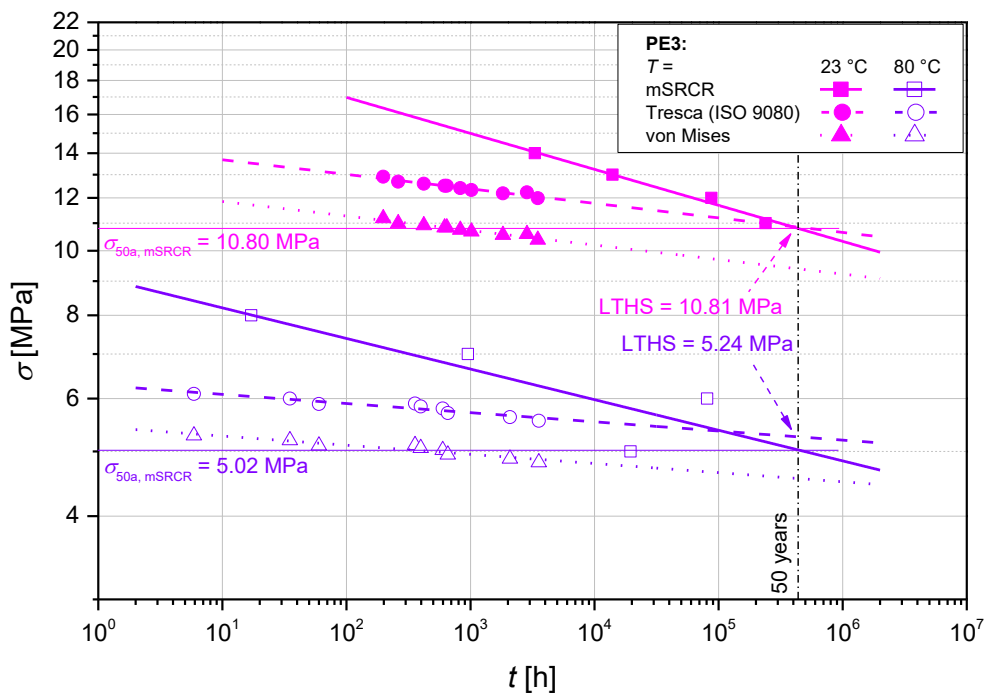


**Fig. 4.22:** Comparison of the mSRCR-test with the equivalent stresses of ISO 9080 for PE2 at  $T = 23$  °C (pink, closed markers) and  $T = 80$  °C (violet, open markers).

## 5 SUMMARY

In this thesis, an accelerated method to predict the long-term behaviour of thermoplastic pipes was attempted. For this purpose, the field of application of the SRCR-test, which has been developed for brittle materials, should be extended to tough materials. Therefore, the dependence of the yield stress on the temperature  $T$  and loading rate must be investigated for the modified SRCR-test (mSRCR). The aim was to define suitable parameters for the measurements of non-reinforced thermoplastics and to modify the evaluation approach.

First, a basic characterization of physical, rheological, thermal and mechanical data via different methods was performed for polyamide 12 (PA12) and polyethylene (PE). Results of the general characterization show no significant deviations from the values in the data sheet, except for tensile test results of PE grades, which showed a considerable deviation of the strain at break ( $\epsilon_b$ ) values, while yield stresses are in good agreement with the datasheets. Still, feasible results were obtained with the mSRCR-test, as – in contrast to the initial method used for brittle materials - within this thesis the yield stress ( $\sigma_{y, \text{mSRCR}}$ ) has been defined as relevant material parameter for extrapolation, and not strain at break ( $\epsilon_{b, \text{mSRCR}}$ ).

The mSRCR-test, was performed on a tensile testing machine at temperatures of  $T = 23 \text{ }^\circ\text{C}$  and  $80 \text{ }^\circ\text{C}$ , respectively. For this purpose, the specific reference stress levels  $\sigma_{\text{ref}}$  and the stress rates  $\dot{\sigma}$  were varied in order to predict a corresponding time until failure  $t_f$ . The physical approach the classical SRCR-test is based has been adopted for plasticity-controlled failure, which predominates in tough materials, since a clear correlation between  $\sigma_{y, \text{mSRCR}}$  and stress rate  $\dot{\sigma}$  as well as  $T$  was confirmed. For the data evaluation within this thesis, a conservative approach has been chosen, considering yielding as relevant failure criterion. Therefore, the mean values of the stress rate-dependent yield stress ( $\sigma_{y, \text{mSRCR}}$ ) and the corresponding time until yielding ( $t_{y, \text{mSRCR}}$ ) were determined and extrapolated to  $\dot{\sigma} = 0 \text{ MPa/s}$  (equals static load conditions). Plotting all predicted  $\sigma_{y, \text{mSRCR}}$  ( $\dot{\sigma} = 0 \text{ MPa/s}$ ) values as a function of predicted  $t_f$  ( $\dot{\sigma} = 0 \text{ MPa/s}$ ) into one diagram, a mSRCR-test based extrapolated Stage I failure curve has been developed which represent the long-term strength behaviour of a specific material under static loading. To improve

predicted results of this method, and to cover the short-term range more precisely, the number of applied  $\sigma_{\text{ref}}$  and  $\dot{\sigma}$  should be increased, especially concerning tests at higher reference stresses. Furthermore, additional standard creep tests at chosen  $\sigma_{\text{ref}}$  should be performed to validate the Stage I failure curves by this method.

The comparison of a uniaxial test (mSRCR) with a multiaxial test (ISO 9080) is limited, due to the different stress states that occur during both tests. Still, with the aid of equivalent stresses, it was possible to compare these methods. For more reliable results, however, the used injection moulded multipurpose specimen for the mSRCR-test should be replaced by tensile specimens milled out of an extruded pipe.

In comparison to the internal pressure pipe test (ISO 9080), which has a test duration of approximately one year, a first overview of the long-term strength behaviour of a material can be made in less than two weeks. However, it should be noted, that this prediction is only valid for multipurpose specimens. With further improvements, the mSRCR method shows a high potential to predict reliable long-term strength behaviour of thermoplastic materials.

## 6 PUBLICATION BIBLIOGRAPHY

Bauwens, J.; Bauwens-Crowet, C.; Homès, G. (1969): Tensile yield-stress behaviour of poly(vinylchloride) and polycarbonate in the glass transition region. In: *J. Polym. Sci. A-2 Polym. Phys.* 7 (10), S. 1745–1754. DOI: 10.1002/pol.1969.160071010.

Bauwens-Crowet, C.; Ots, J.-M.; Bauwens, J.-C. (1974): The strain-rate and temperature dependence of yield of polycarbonate in tension, tensile creep and impact tests. In: *J Mater Sci* 9 (7), S. 1197–1201. DOI: 10.1007/BF00552841.

Böge, A.; Böge, W. (2017): Technische Mechanik. Statik - Reibung - Dynamik - Festigkeitslehre - Fluidmechanik. 32., überarbeitete und erweiterte Auflage. Wiesbaden: Springer Vieweg (Lehrbuch).

Bonten, C. (2016): Kunststofftechnik. Einführung und Grundlagen. 2. Aufl. München: Carl Hanser Verlag.

Bowden, P.; Young, R. (1974): Deformation mechanisms in crystalline polymers. In: *J Mater Sci* 9 (12), S. 2034–2051. DOI: 10.1007/BF00540553.

Brömstrup, H. (Hg.) (2009): PE 100 pipe systems. 3. ed. Essen: Vulkan-Verl.

Bueche, F. (1957): Tensile Strength of Plastics below the Glass Temperature. In: *Journal of Applied Physics* 28 (7), S. 784–787. DOI: 10.1063/1.1722855.

Bueche, F. (1958): Tensile Strength of Plastics: Effects of Flaws and Chain Relaxation. In: *Journal of Applied Physics* 29 (8), S. 1231–1234. DOI: 10.1063/1.1723408.

Domininghaus, H.; Elsner, P.; Eyerer, P.; Hirth, T. (Hg.) (2012): Kunststoffe. Eigenschaften und Anwendungen. 8., neu bearb. und erw. Aufl. Berlin, Heidelberg: Springer (VDI-Buch).

Ehrenstein, G.; Riedel, G.; Trawiel, P. (2003): Praxis der Thermischen Analyse von Kunststoffen. 2., völlig überarb. Aufl. München: Hanser.



- Eyring, H. (1936): Viscosity, Plasticity, and Diffusion as Examples of Absolute Reaction Rates. In: *The Journal of Chemical Physics* 4 (4), S. 283. DOI: 10.1063/1.1749836.
- Frank, A.; Pinter, G. (2014): Evaluation of the applicability of the cracked round bar test as standardized PE-pipe ranking tool. In: *Polym Test* 33, S. 161–171. DOI: 10.1016/j.polymertesting.2013.11.013.
- Gloggnitzer, S.; Guttman, P.; Pinter, G. (Hg.) (2018): Accelerated Approaches for Life-Time Prediction of Composites under Static Loads. ECCM18 - 18th European Conference on Composite Materials. Athens, Greece, 22-28th June.
- Grellmann, W.; Seidler, S. (Hg.) (2011): Kunststoffprüfung. 2. Auflage. München: Carl Hanser Verlag.
- Haager, M. (2006): Bruchmechanische Methoden zur beschleunigten Charakterisierung des langsamen Risswachstums von Polyethylen-Rohrwerkstoffen. Dissertation. University of Leoben, Leoben, Austria.
- Halpin, J. (1964): Fracture of Amorphous Polymeric Solids: Time to Break. In: *Journal of Applied Physics* 35 (11), S. 3133–3141. DOI: 10.1063/1.1713191.
- Halpin, J.; Bueche, F. (1964): Fracture of Amorphous Polymeric Solids: Reinforcement. In: *Journal of Applied Physics* 35 (11), S. 3142–3149. DOI: 10.1063/1.1713192.
- Hartmann, M. (2014): Polyamid 12-Rohre im Gas-Hochdruckbereich 2014, Juni 2014. available online at <https://www.vestamid.com/product/peek-industrial/downloads/krv-pa12-rohre-im-gas-hochdruckbereich-de.pdf>, checked on 12.02.2020.
- Hiss, R.; Hobeika, S.; Lynn, C.; Strobl, G. (1999): Network Stretching, Slip Processes, and Fragmentation of Crystallites during Uniaxial Drawing of Polyethylene and Related Copolymers. A Comparative Study. In: *Macromolecules* 32 (13), S. 4390–4403. DOI: 10.1021/ma981776b.
- Jar, B. (Hg.) (2019): Determining Critical Stress for Ductile-Brittle Transition of Polyethylene Pipe Under Creep Loading. ANTEC. Orlando, FL, USA. In proc: Annual Technical Conference - ANTEC.

Kanters, M. (2015): Prediction of Long-Term Performance of Load-Bearing Thermoplastics. Ph.D. Thesis. Technische Universiteit Eindhoven, Eindhoven, NL.

Kanters, M.; Remerie, K.; Govaert, L. (2016): A new protocol for accelerated screening of long-term plasticity-controlled failure of polyethylene pipe grades. In: *Polym Eng Sci* 56 (6), S. 676–688. DOI: 10.1002/pen.24294.

Kinloch, A.; Young, R. (1995): Fracture Behaviour of Polymers. Dordrecht: Springer Netherlands.

Klompen, E.T.J.; Govaert, L. (1999): Nonlinear Viscoelastic Behaviour of Thermorheologically Complex Materials. In: *Mechanics of Time-Dependent Materials* 3 (1), S. 49–69. DOI: 10.1023/A:1009853024441.

Lang, R.; Pinter, G.; Balika, W. (2005): Qualification concept for lifetime assessment of PE pressure pipes for arbitrary installation conditions. Konzept zur Nachweisführung für Nutzungsdauer und Sicherheit von PE-Druckrohren bei beliebiger Einbausituation. In: *3R international* 44 (1-2), S. 33–41.

Lang, R.; Stern, A.; Dörner, G. (1997): Applicability and limitations of current lifetime prediction models for thermoplastics pipes under internal pressure. In: *Angew Makromol Chemie* 247 (1), S. 131–145. DOI: 10.1002/apmc.1997.052470109.

Pepels, M. (2015): Exploring the potential of polymacrolactones as polyethylene-mimics. Ph.D. Thesis. Technische Universiteit Eindhoven, Eindhoven, NL.

Pinter, G. (1999): Reißwachstumsverhalten von PE-HD unter statischer Belastung. Dissertation. Montanuniversität Leoben, Leoben.

ISO 527, 2012: Plastics -- Determination of tensile properties.

ISO 1133, 2005: Plastics -- Determination of the melt mass-flow rate (MFR) and the melt volume-flow rate (MVR) of thermoplastics.

ISO 11357, 2002: Plastics -- Differential scanning calorimetry (DSC).

ISO 1183, 2012: Plastics -- Methods for determining the density of non-cellular plastics.

ISO 9080, 2012: Plastics piping and ducting systems -- Determination of the long-term hydrostatic strength of thermoplastics materials in pipe form by extrapolation.

ISO 18489, 2015: Polyethylene (PE) materials for piping systems -- Determination of resistance to slow crack growth under cyclic loading -- Cracked Round Bar test method.

Redhead, A. (2009): Zyklische Risswachstumsversuche an CRB-Proben als Qualitätssicherungstest zur Abschätzung des Langzeitverhaltens von PE-Rohrwerkstoffen. Masterarbeit. Montanuniversität, Leoben.

Ree, T.; Eyring, H. (1955): Theory of Non-Newtonian Flow. I. Solid Plastic System. In: *J. Appl. Phys.* 26 (7), S. 793. DOI: 10.1063/1.1722098.

Roetling, J.A. (1966): Yield stress behaviour of isotactic polypropylene. In: *Polymer* 7 (7), S. 303–306. DOI: 10.1016/0032-3861(66)90025-5.

Tan, N.; Jar, P.-Y. (Hg.) (2019): Multi-Relaxation Test to Characterize PE Pipe Performance. In proc: Annual Technical Conference - ANTEC. Detroit, MI, USA.

ASTM D2837, 2013: Test Method for Obtaining Hydrostatic Design Basis for Thermoplastic Pipe Materials or Pressure Design Basis for Thermoplastic Pipe Products.

van Erp, T.; Cavallo, D.; Peters, G.; Govaert, L. (2012): Rate-, temperature-, and structure-dependent yield kinetics of isotactic polypropylene. In: *J. Polym. Sci. B Polym. Phys.* 50 (20), S. 1438–1451. DOI: 10.1002/polb.23150.

Visser, H.; Bor, T.; Wolters, M.; Engels, T.; Govaert, L. (2010): Lifetime Assessment of Load-Bearing Polymer Glasses: An Analytical Framework for Ductile Failure. In: *Macromol. Mater. Eng.* 295 (7), S. 637–651. DOI: 10.1002/mame.200900369.

Wunderlich, B. (2005): Thermal Analysis of Polymeric Materials. Berlin, Heidelberg: Springer-Verlag Berlin Heidelberg. available online at <http://site.ebrary.com/lib/alltitles/docDetail.action?docID=10229032>.

Zhou, W.; Chudnovsky, A.; Bosnyak, C.; Sehanobish, K. (1999): The Time Dependency of the Necking Process in Polyethylene. In: Proceedings. Annual

Technical Conference - ANTEC. New York, New York, USA. Society of Plastics Engineers, S. 3399–3403.

Zhou, W.; Chudnovsky, A.; Sehanobish, K. (Hg.) (2005): Evaluation of Time to Ductile Failure in Creep of PEs from Short-term Testing. ANTEC.

Zhurkov, S. (1965): Kinetic Concept of the Strength of Solids. In: *International Journal of Fracture Mechanics* (1:4), S. 311–323.

Zhurkov, S.; Tomashevsky, E. (Hg.) (1966): Physical basis of yield and fracture. London. Institute of Physics: Oxford U.P.